institutions within a single country. The good outcomes for HCC seen in Japan[9] compared with those in Europe[54] and the USA[55] are the result of the meticulous medical care for HCC that has been practiced in Japan.

REFERENCES

1 Kudo M, Izumi N, Kokudo N *et al.* Management of hepatocellular carcinoma in Japan: Consensus-Based Clinical Practice Guidelines proposed by the Japan Society of Hepatology (JSH) 2010 updated version. *Dig Dis* 2011; **29**: 339–64.
2 Clinical Practice Guidelines for hepatocellular carcinoma – The Japan Society of Hepatology 2009 update. *Hepatol Res* 2010; **40** (Suppl 1): 2–144.
3 Kishi Y, Saiura A, Yamamoto J *et al.* Significance of anatomic resection for early and advanced hepatocellular carcinoma. *Langenbecks Arch Surg* 2012; **397**: 85–92.
4 Wakai T, Shirai Y, Sakata J *et al.* Anatomic resection independently improves long-term survival in patients with T1-T2 hepatocellular carcinoma. *Ann Surg Oncol* 2007; **14**: 1356–65.
5 Makuuchi M, Hasegawa H, Yamazaki S. Indication for hepatectomy in patients with hepatocellular carcinoma and cirrhosis (in Japanese). *Shindan to Chiryo* 1986; **1986**: 1225–30.
6 Kaibori M, Ha-Kawa SK, Maehara M *et al.* Usefulness of Tc-99m-GSA scintigraphy for liver surgery. *Ann Nucl Med* 2011; **25**: 593–602.
7 Nanashima A, Abo T, Tobinaga S *et al.* Prediction of indocyanine green retention rate at 15 minutes by correlated liver function parameters before hepatectomy. *J Surg Res* 2011; **169**: e119–25.
8 Arii S, Sata M, Sakamoto M *et al.* Management of hepatocellular carcinoma: report of Consensus Meeting in the 45th Annual Meeting of the Japan Society of Hepatology (2009). *Hepatol Res* 2010; **40**: 667–85.
9 Ikai I, Kudo M, Arii S *et al.* Report of the 18th follow-up survey of primary liver cancer in Japan. *Hepatol Res* 2010; **40**: 1043–59.
10 Ueno S, Sakoda M, Kurahara H *et al.* Preoperative segmentation of the liver, based on 3D CT images, facilitates laparoscopic anatomic hepatic resection for small nodular hepatocellular carcinoma in patients with cirrhosis. *Hepatogastroenterology* 2010; **57**: 807–12.
11 Suzuki H, Shimura T, Suehiro T *et al.* Laparoscopic partial liver resection for hepatocellular carcinoma in liver cirrhosis. *Hepatogastroenterology* 2008; **55**: 2228–32.
12 Kaneko H, Takagi S, Otsuka Y *et al.* Laparoscopic liver resection of hepatocellular carcinoma. *Am J Surg* 2005; **189**: 190–4.
13 Kitisin K, Packiam V, Bartlett DL, Tsung A. A current update on the evolution of robotic liver surgery. *Minerva Chir* 2011; **66**: 281–93.
14 Ku Y, Iwasaki T, Tominaga M *et al.* Reductive surgery plus percutaneous isolated hepatic perfusion for multiple advanced hepatocellular carcinoma. *Ann Surg* 2004; **239**: 53–60.
15 Liver transplantation in Japan – registry by the Japanese Liver Transplantation Society – (in Japanese) – registry by the Japanese Liver Transplantation Society-. *Ishoku* 2010; **45**: 621–32.
16 Sakaguchi T, Suzuki S, Morita Y *et al.* Impact of the preoperative des-gamma-carboxy prothrombin level on prognosis after hepatectomy for hepatocellular carcinoma meeting the Milan criteria. *Surg Today* 2010; **40**: 638–45.
17 Hasegawa K, Imamura H, Ijichi M *et al.* Inclusion of tumor markers improves the correlation of the Milan criteria with vascular invasion and tumor cell differentiation in patients with hepatocellular carcinoma undergoing liver resection (#JGSU-D-07-00462). *J Gastrointest Surg* 2008; **12**: 858–66.
18 Matsuno N, Iwamoto H, Nakamura Y *et al.* ABO-incompatible adult living donor liver transplantation for hepatocellular carcinoma. *Transplant Proc* 2008; **40**: 2497–500.
19 Shiina S, Teratani T, Obi S *et al.* A randomized controlled trial of radiofrequency ablation with ethanol injection for small hepatocellular carcinoma. *Gastroenterology* 2005; **129**: 122–30.
20 Lin SM, Lin CJ, Lin CC, Hsu CW, Chen YC. Radiofrequency ablation improves prognosis compared with ethanol injection for hepatocellular carcinoma < or =4 cm. *Gastroenterology* 2004; **127**: 1714–23.
21 Lencioni RA, Allgaier HP, Cioni D *et al.* Small hepatocellular carcinoma in cirrhosis: randomized comparison of radio-frequency thermal ablation versus percutaneous ethanol injection. *Radiology* 2003; **228**: 235–40.
22 Bouza C, Lopez-Cuadrado T, Alcazar R, Saz-Parkinson Z, Amate JM. Meta-analysis of percutaneous radiofrequency ablation versus ethanol injection in hepatocellular carcinoma. *BMC Gastroenterol* 2009; **9**: 31.
23 Asahina Y, Nakanishi H, Izumi N. Laparoscopic radiofrequency ablation for hepatocellular carcinoma. *Dig Endosc* 2009; **21**: 67–72.
24 Inoue T, Minami Y, Chung H *et al.* Radiofrequency ablation for hepatocellular carcinoma: assistant techniques for difficult cases. *Oncology* 2010; **78** (Suppl 1): 94–101.
25 Uehara T, Hirooka M, Ishida K *et al.* Percutaneous ultrasound-guided radiofrequency ablation of hepatocellular carcinoma with artificially induced pleural effusion and ascites. *J Gastroenterol* 2007; **42**: 306–11.
26 Rhim H, Lim HK. Radiofrequency ablation for hepatocellular carcinoma abutting the diaphragm: the value of artificial ascites. *Abdom Imaging* 2009; **34**: 371–80.
27 Rhim H, Lim HK, Kim YS, Choi D. Percutaneous radiofrequency ablation with artificial ascites for hepatocellular carcinoma in the hepatic dome: initial experience. *AJR Am J Roentgenol* 2008; **190**: 91–8.

28 Song I, Rhim H, Lim HK, Kim YS, Choi D. Percutaneous radiofrequency ablation of hepatocellular carcinoma abutting the diaphragm and gastrointestinal tracts with the use of artificial ascites: safety and technical efficacy in 143 patients. *Eur Radiol* 2009; **19**: 2630–40.
29 Ogawa T, Kawamoto H, Kobayashi Y *et al.* Prevention of biliary complication in radiofrequency ablation for hepatocellular carcinoma-Cooling effect by endoscopic nasobiliary drainage tube. *Eur J Radiol* 2010; **73**: 385–90.
30 Masuzaki R, Shiina S, Tateishi R *et al.* Utility of contrast-enhanced ultrasonography with Sonazoid in radiofrequency ablation for hepatocellular carcinoma. *J Gastroenterol Hepatol* 2011; **26**: 759–64.
31 Miyamoto N, Hiramatsu K, Tsuchiya K, Sato Y, Terae S, Shirato H. Sonazoid-enhanced sonography for guiding radiofrequency ablation for hepatocellular carcinoma: better tumor visualization by Kupffer-phase imaging and vascular-phase imaging after reinjection. *Jpn J Radiol* 2009; **27**: 185–93.
32 Nakai M, Sato M, Sahara S *et al.* Radiofrequency ablation assisted by real-time virtual sonography and CT for hepatocellular carcinoma undetectable by conventional sonography. *Cardiovasc Intervent Radiol* 2009; **32**: 62–9.
33 Matsui O, Kadoya M, Yoshikawa J *et al.* Small hepatocellular carcinoma: treatment with subsegmental transcatheter arterial embolization. *Radiology* 1993; **188**: 79–83.
34 Matsui O, Kadoya M, Yoshikawa J, Gabata T, Takashima T, Demachi H. Subsegmental transcatheter arterial embolization for small hepatocellular carcinomas: local therapeutic effect and 5-year survival rate. *Cancer Chemother Pharmacol* 1994; **33** (Suppl): S84–8.
35 Takayasu K, Arii S, Kudo M *et al.* Superselective transarterial chemoembolization for hepatocellular carcinoma. Validation of treatment algorithm proposed by Japanese guidelines. *J Hepatol* 2012; **56**: 886–92.
36 Okabe K, Beppu T, Haraoka K *et al.* Safety and short-term therapeutic effects of miriplatin-lipiodol suspension in transarterial chemoembolization (TACE) for hepatocellular carcinoma. *Anticancer Res* 2011; **31**: 2983–8.
37 Okusaka T, Kasugai H, Ishii H *et al.* A randomized phase II trial of intra-arterial chemotherapy using SM-11355 (Miriplatin) for hepatocellular carcinoma. *Invest New Drugs* 2011; doi. 10.1007/s10637-011-9776-4.
38 Takayasu K. Chemoembolization for unresectable hepatocellular carcinoma in Japan. *Oncology* 2010; **78** (Suppl 1): 135–41.
39 Nagano H, Miyamoto A, Wada H *et al.* Interferon-alpha and 5-fluorouracil combination therapy after palliative hepatic resection in patients with advanced hepatocellular carcinoma, portal venous tumor thrombus in the major trunk, and multiple nodules. *Cancer* 2007; **110**: 2493–501.
40 Nagano H, Wada H, Kobayashi S *et al.* Long-term outcome of combined interferon-alpha and 5-fluorouracil treatment for advanced hepatocellular carcinoma with major portal vein thrombosis. *Oncology* 2011; **80**: 63–9.
41 Furuse J, Ishii H, Nakachi K, Suzuki E, Shimizu S, Nakajima K. Phase I study of sorafenib in Japanese patients with hepatocellular carcinoma. *Cancer Sci* 2008; **99**: 159–65.
42 Kaneko S, Furuse J, Kudo M *et al.* Guideline on th euse if new anticancer drugs for the treatment of Hepatocellular Carcinoma 2010 update. *Hepatol Res* 2012 (in press).
43 Monden M, Sakon M, Sakata Y, Ueda Y, Hashimura E. 5-fluorouracil arterial infusion + interferon therapy for highly advanced hepatocellular carcinoma: a multicenter, randomized, phase II study. *Hepatol Res* 2012; **42**: 150–65.
44 Obi S, Yoshida H, Toune R *et al.* Combination therapy of intraarterial 5-fluorouracil and systemic interferon-alpha for advanced hepatocellular carcinoma with portal venous invasion. *Cancer* 2006; **106**: 1990–7.
45 Yamashita T, Arai K, Sunagozaka H *et al.* Randomized, Phase II Study comparing interferon combined with hepatic arterial infusion of fluorouracil plus cisplatin and fluorouracil alone in patients with advanced hepatocellular carcinoma. *Oncology* 2011; **81**: 281–90.
46 Ueshima K, Kudo M, Takita M *et al.* Hepatic arterial infusion chemotherapy using low-dose 5-fluorouracil and cisplatin for advanced hepatocellular carcinoma. *Oncology* 2010; **78** (Suppl 1): 148–53.
47 Ando E, Tanaka M, Yamashita F *et al.* Hepatic arterial infusion chemotherapy for advanced hepatocellular carcinoma with portal vein tumor thrombosis: analysis of 48 cases. *Cancer* 2002; **95**: 588–95.
48 Tanioka H, Tsuji A, Morita S *et al.* Combination chemotherapy with continuous 5-fluorouracil and low-dose cisplatin infusion for advanced hepatocellular carcinoma. *Anticancer Res* 2003; **23**: 1891–7.
49 Chung YH, Song IH, Song BC *et al.* Combined therapy consisting of intraarterial cisplatin infusion and systemic interferon-alpha for hepatocellular carcinoma patients with major portal vein thrombosis or distant metastasis. *Cancer* 2000; **88**: 1986–91.
50 McIntosh A, Hagspiel KD, Al-Osaimi AM *et al.* Accelerated treatment using intensity-modulated radiation therapy plus concurrent capecitabine for unresectable hepatocellular carcinoma. *Cancer* 2009; **115**: 5117–25.
51 Komatsu S, Fukumoto T, Demizu Y *et al.* Clinical results and risk factors of proton and carbon ion therapy for hepatocellular carcinoma. *Cancer* 2011; **117**: 4890–904.
52 Sugahara S, Oshiro Y, Nakayama H *et al.* Proton beam therapy for large hepatocellular carcinoma. *Int J Radiat Oncol Biol Phys* 2010; **76**: 460–6.
53 Yoshida H, Shiratori Y, Kudo M *et al.* Effect of vitamin K2 on the recurrence of hepatocellular carcinoma. *Hepatology* 2011; **54**: 532–40.
54 Berrino F, De Angelis R, Sant M *et al.* Survival for eight major cancers and all cancers combined for European adults diagnosed in 1995–99: results of the EUROCARE-4 study. *Lancet Oncol* 2007; **8**: 773–83.
55 Siegel R, Naishadham D, Jemal A. Cancer statistics, 2012. *CA Cancer J Clin* 2012; **62**: 10–29.

Biochemical and Biophysical Research Communications 441 (2013) 230–235

Contents lists available at ScienceDirect

Biochemical and Biophysical Research Communications

journal homepage: www.elsevier.com/locate/ybbrc

A novel TK-NOG based humanized mouse model for the study of HBV and HCV infections

Keiichi Kosaka [a,b], Nobuhiko Hiraga [a,b], Michio Imamura [a,b], Satoshi Yoshimi [a,b], Eisuke Murakami [a,b], Takashi Nakahara [a,b], Yoji Honda [a,b], Atsushi Ono [a,b], Tomokazu Kawaoka [a,b], Masataka Tsuge [a,b], Hiromi Abe [a,b], C. Nelson Hayes [a,b,c], Daiki Miki [b,c], Hiroshi Aikata [a,b], Hidenori Ochi [b,c], Yuji Ishida [b,d], Chise Tateno [b,d], Katsutoshi Yoshizato [b,d], Tamito Sasaki [a,b], Kazuaki Chayama [a,b,c,*]

[a] Department of Gastroenterology and Metabolism, Applied Life Sciences, Institute of Biomedical & Health Science, Hiroshima University, Hiroshima, Japan
[b] Liver Research Project Center, Hiroshima University, Hiroshima, Japan
[c] Laboratory for Digestive Diseases, Center for Genomic Medicine, The Institute of Physical and Chemical Research (RIKEN), Hiroshima, Japan
[d] PhoenixBio Co., Ltd., Higashihiroshima, Japan

ARTICLE INFO

Article history:
Received 20 September 2013
Available online 16 October 2013

Keywords:
Human hepatocyte chimeric mouse
TK-NOG mouse
uPA–SCID mouse
Hepatitis B virus
Hepatitis C virus
Human serum albumin

ABSTRACT

The immunodeficient mice transplanted with human hepatocytes are available for the study of the human hepatitis viruses. Recently, human hepatocytes were also successfully transplanted in herpes simplex virus type-1 thymidine kinase (TK)-NOG mice. In this study, we attempted to infect hepatitis virus in humanized TK-NOG mice and urokinase-type plasminogen activator-severe combined immunodeficiency (uPA–SCID) mice. TK-NOG mice were injected intraperitoneally with 6 mg/kg of ganciclovir (GCV), and transplanted with human hepatocytes. Humanized TK-NOG mice and uPA/SCID mice were injected with hepatitis B virus (HBV)- or hepatitis C virus (HCV)-positive human serum samples. Human hepatocyte repopulation index (RI) estimated from human serum albumin levels in TK-NOG mice correlated well with pre-transplantation serum ALT levels induced by ganciclovir treatment. All humanized TK-NOG and uPA–SCID mice injected with HBV infected serum developed viremia irrespective of lower replacement index. In contrast, establishment of HCV viremia was significantly more frequent in TK-NOG mice with low human hepatocyte RI (<70%) than uPA–SCID mice with similar RI. Frequency of mice spontaneously in early stage of viral infection experiment (8 weeks after injection) was similar in both TK-NOG mice and uPA–SCID mice. Effects of drug treatment with entecavir or interferon were similar in both mouse models. TK-NOG mice thus useful for study of hepatitis virus virology and evaluation of anti-viral drugs.

1. Introduction

Hepatitis B virus (HBV) and hepatitis C virus (HCV) infections are serious health problems worldwide. More than 350 and 170 million people are infected with HBV and HCV, respectively [1,2]. Both types of hepatitis viruses result in the development of chronic liver infection and potentially death due to liver failure and hepatocellular carcinoma [3]. Although the chimpanzee is a useful animal model for the study of HBV and HCV infection, there are ethical restrictions and hampered by the high financial cost on the use of this animal. The immunodeficient mice with a urokinase-type plasminogen activator (uPA) transgene [4,5] or a targeted disruption of the murine fumaryl acetoacetate hydrolase (FAH) [6–10] were shown to be excellent recipients for human hepatocyte. These small animal models are available for hepatitis viruses infection [4,11], and are useful for the study of HBV and HCV biology [12–14]. However, there are disadvantages that limit the utility of this model for many applications, including excessive mortality [9].

Recently, human hepatocytes were successfully transplanted into severely immunodeficient NOG mice with the herpes simplex virus type-1 thymidine kinase (HSVtk) expressing in mouse hepatocytes (TK-NOG) [15]. Mouse liver cells expressing HSVtk

Abbreviations: ALT, alanine aminotransferase; GCV, ganciclovir; HBV, hepatitis B virus; HCV, hepatitis C virus; HSA, human serum albumin; HSVtk, herpes simplex virus type-1 thymidine kinase; IFN, interferon; PegIFN-alpha, pegylated interferon-alpha; RI, repopulation index; RT-PCR, reverse transcript-polymerase chain reaction; SCID, severe combined immunodeficiency; uPA, urokinase-type plasminogen activator.

* Corresponding author. Address: Department of Gastroenterology and Metabolism, Applied Life Sciences, Institute of Biomedical & Health Sciences, Hiroshima University, 1-2-3 Kasumi, Minami-ku, Hiroshima 734-8551, Japan. Fax: +81 82 255 6220.
E-mail address: chayama@hiroshima-u.ac.jp (K. Chayama).

0006-291X/$ - see front matter © 2013 Elsevier Inc. All rights reserved.
http://dx.doi.org/10.1016/j.bbrc.2013.10.040

were ablated after a brief exposure to ganciclovir (GCV), and transplanted human hepatocytes were stably maintained within the mouse liver without exogenous drug administration [15]. The analyses of drug interactions and pharmacokinetics have previously been reported using TK-NOG mice transplanted with human hepatocytes [15–18]. In the present study, we succeeded in infecting human hepatocyte-transplanted TK-NOG mice with HBV and HCV and showed that this mouse model is as useful as the uPA/SCID model for the study of hepatitis viruses.

2. Materials and methods

2.1. Animal treatment

TK-NOG mice were purchased from Central Institute for Experimental Animals (CIEA, Kawasaki, Japan). Eight-weeks-old mice were injected intraperitoneally with 6 mg/kg of GCV twice a day. After two days, mice were re-injected with the same amount of GCV. Seven days after 1st GCV injection, mice were transplanted with 1 or 2 $\times$ 10^6 of human hepatocytes obtained from human hepatocyte transplanted uPA–SCID chimeric mice by collagenase perfusion method by intra-splenic injection. Transplanted human hepatocytes used in this study were obtained from a same donor. One week after the first GCV treatment, serum alanine aminotransferase (ALT) levels were measured (Fuji DRI-CHEM, Fuji Film, Tokyo, Japan). Infection, extraction of serum samples, and sacrifice were performed under ether anesthesia. Mouse serum concentration of human serum albumin (HSA), which correlated with the human hepatocyte repopulation index (RI) [15], was measured as previously described [5]. Generation of the uPA/SCID mice and transplantation of human hepatocytes were performed as described previously [5,12,19]. The experimental protocol was approved by the Ethics Review Committee for Animal Experimentation of the Graduate School of Biomedical Sciences, Hiroshima University.

2.2. Human serum samples

Human serum samples containing high titers of either genotype C HBV (5.3 $\times$ 10^6 copies/mL) or genotype 1b HCV (2.2 $\times$ 10^6 copies/mL) were obtained from patients with chronic hepatitis who provided written informed consent. The individual serum samples were divided into small aliquots and stored separately in liquid nitrogen until use. Mice were injected intravenously with 50 μL of either HBV- or HCV-positive human serum. The study protocol conforms to the ethical guidelines of the 1975 Declaration of Helsinki and was approved a priori by the institutional review committee.

2.3. Quantitation of HBV and HCV

DNA and RNA extraction and quantitation of HBV and HCV by real-time polymerase chain reaction (RT-PCR) were performed as described previously [12,13,19]. Briefly, DNA was extracted using SMITEST (Genome Science Laboratories, Tokyo, Japan) and dissolved in 20 μL H_2O, and RNA was extracted from serum samples using SepaGene RVR (Sankojunyaku, Tokyo, Japan) and reverse transcribed with a random hexamer and a reverse transcriptase (ReverTraAce; TOYOBO, Osaka, Japan) according to the instructions provided by the manufacturer. Quantitation of HBV DNA and HCV RNA was performed using Light Cycler (Roche Diagnostic, Japan, Tokyo). The lower detection limits of real-time PCR for HBV DNA and HCV RNA are 4.4 and 3.5 log copies/mL, respectively.

2.4. Histochemical analysis of mouse liver

Liver specimens of HBV-infected TK-NOG mice were fixed with 10% buffered-paraformaldehyde and embedded in paraffin blocks for histological examination. Hematoxylin-eosin and immunohistochemical staining using antibodies against HSA (Bethyl Laboratories Inc., Montgomery, TX) and hepatitis B core antigen (HBc-Ag) (DAKO Diagnostika, Hamburg, Germany) were performed as described previously [12].

2.5. Treatment with antiviral agents

Mice were treated with antiviral agents eight weeks after HBV or HCV infection, by which time stable viremia had developed. HBV-infected mice were administered either food containing 0.3 mg of entecavir/kg of body weight/day or daily intramuscular injections with 7000 IU/kg of IFN-alpha (Otsuka Pharmaceutical Co., Ltd., Tokyo, Japan). HCV-infected mice were administered intramuscular injection with either 1000 IU/kg of IFN-alpha daily or 10 μg/kg of PegIFN-alpha-2a (Chugai Pharmaceutical Co., Ltd., Tokyo, Japan) twice a week for three weeks.

2.6. Statistical analysis

Differences in HSA levels between TK-NOG mice and uPA–SCID mice, and incidence of infection between highly and poorly repopulated mice were examined for statistical significance using the Mann–Whitney *U*-test.

3. Results

3.1. Correlation between serum ALT level after GCV administration and the human hepatocyte index in TK-NOG mice

We analyzed the correlation between serum ALT levels after GCV injection and the human hepatocyte RI using 194 TK-NOG mice. Seven days after GCV injection when serum ALT levels had reached maximum levels [15], mice were transplanted with human hepatocytes. After transplantation of human hepatocytes, serum concentrations of HSA increased and reached plateau at 6–8 weeks. Serum ALT levels one week after GCV administration and HSA levels 8 weeks after hepatocyte transplantation showed a positive correlation, indicating that the higher serum ALT level, the higher the RI (Fig. 1A). HSA levels 8 weeks after human hepatocyte transplantation in TK-NOG mice were lower than in uPA–SCID mice (Fig 1B), which indicates that mice livers were more efficiently replaced with human hepatocytes in uPA–SCID mice than in TK-NOG mice.

3.2. Infection with hepatitis viruses in humanized TK-NOG mice and uPA–SCID mice

Eight weeks after human hepatocyte transplantation, TK-NOG mice and uPA–SCID mice with HSA levels over 1.0 mg/mL were inoculated with either HBV- or HCV-positive human serum samples. Eight weeks after injection, the frequency of the development of viremia was compared between the mice with lower (<70%) and higher ($\geqslant$70%) human hepatocyte RI. 70% of RI corresponds to 5.4 and 6.3 mg/dl of serum HAS in TK-NOG mice and uPA–SCID mice, respectively [5,15]. All humanized TK-NOG and uPA–SCID mice inoculated with HBV developed viremia 8 weeks after injection, irrespective of the RI (Fig. 2A). Incidence of HCV viremia was also high in TK-NOG mice regardless of the RI. In contrast, the frequency of HCV viremia was much lower in uPA–SCID mice with the RI. Only 20% (1 of 5) of uPA–SCID mice with low RI became

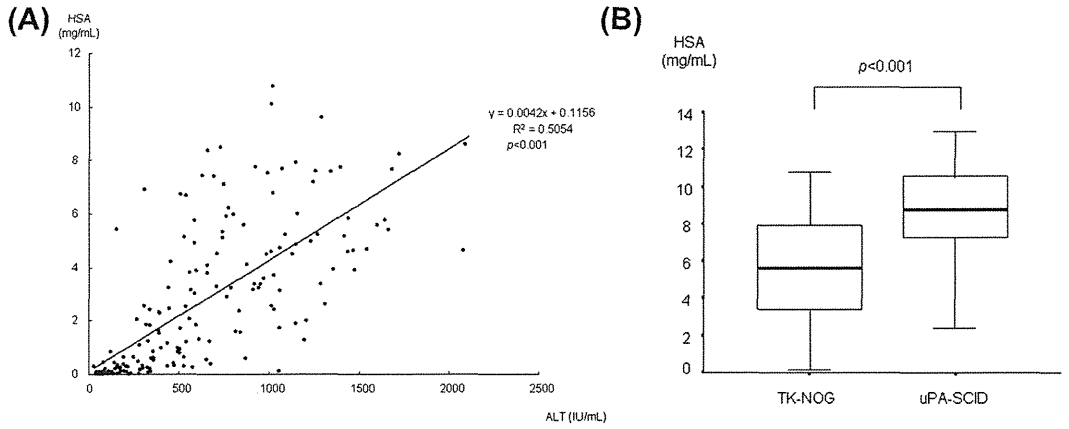

Fig. 1. Human hepatocyte repopulation index in humanized mice. Serum alaninaminotransferase (ALT) levels in TK-NOG mice were measured one week after ganciclovir treatment. Human serum albumin (HSA) levels were measured eight weeks after transplantation of human hepatocytes. (A) Correlation between serum ALT level after ganciclovir administration and human hepatocyte repopulation index in TK-NOG mice. Points represent single mouse measurements. *r* (Spearman rank) and *P* value are shown. (B) HSA levels in TK-NOG mice and uPA–SCID mice. In these box-and-whisker plots, lines within the boxes represent median values; the upper and lower lines of the boxes represent the 25th and 75th percentiles, respectively; and the upper and lower bars outside the boxes represent the 90th and 10th percentiles, respectively.

positive for HCV, whereas 94.3% (50 of 53) of mice with high RI became positive ($p = 1.07 \times 10^{-6}$). Serum viral titers gradually increased in mice that developed viremia. Eight weeks after infection, HBV DNA and HCV RNA titers increased to approximately 8 and 6 log copies/mL, respectively in both TK-NOG and uPA–SCID mice (Fig. 2B). Viremia levels were slightly higher in uPA–SCID mice than TK-NOG mice, probably due to higher human hepatocyte RI (HSA levels) in uPA–SCID mice. In HBV-infected TK-NOG mice, histological analysis showed that hepatocytes positive for HSA were also positive for HB core antigen (Fig. 2C), which is in line with our previous findings using uPA–SCID mice [12].

3.3. The effect of antiviral agents on hepatitis virus-infected humanized mice

We analyzed the effect of antiviral agents on HBV- and HCV-infected humanized mice. Eight weeks after HBV-infection, 2 humanized TK-NOG mice were orally administrated 0.3 mg/kg day of entecavir, and 2 other mice received intramuscular injections with 7000 IU/g of IFN-alpha daily for 3 weeks. Both treatments resulted in a rapid reduction of mouse serum HBV DNA titers (Fig. 3A). Two HCV-infected humanized TK-NOG mice were administrated IFN-alpha daily, and 2 other mice received PegIFN-alpha-2a injections twice a week for 3 weeks. Both treatments resulted in a reduction of HCV RNA titers in mouse serum. The effects of these antiviral agents on HBV and HCV in TK-NOG mice were similar to those in uPA–SCID mice (Fig. 3B).

3.4. Incidence of unexpected death

The incidence of unexpected death is high in human hepatocyte chimeric uPA–SCID mice [20]. Incidence of unexpected death in the early stages of viral infection (within 8 weeks of viral infection) was similar between TK-NOG mice and uPA–SCID mice (6.3% vs 10.6%, $p = 0.465$) (Fig. 4).

4. Discussion

Human hepatocyte chimeric mice are valuable tool for hepatitis virology and drug assessment [12–14]. To establish human hepatocyte chimerism, two conditions are necessary: immunodeficiency and mouse-specific liver cell damage. For immune deficiency, SCID mice [4,5,12–14,20], NOG mice [8,21] and RAG-2 deficient mice [6,9,10] have been reported. We previously reported that the level of immunodeficiency in SCID mice, which are the most weakly immunodeficient of the three types, is sufficient to prevent rejection of transplanted human hepatocytes [5]. However, preventive treatments for human liver cell rejection via mice NK cells, such as an anti-asialo GM1 antibody, are necessary in SCID mice [5].

To evoke mouse liver cell injury, uPA and FAH transgene techniques were used [4–10]. Recently, successful human liver cell transplantation to TK-NOG mice in the absence of ongoing drug treatment after a brief exposure to a non-toxic dose of GCV has been reported [15]. We thus attempted to use TK-NOG mice to establish high levels of replacement with human hepatocytes and tried to infect hepatitis viruses.

In this study, we transplanted human hepatocytes to 194 TK-NOG mice and analyzed whether elevated serum ALT levels, which results from liver damage caused by GCV exposure, reflects HSA levels, as it is known that HSA levels are correlated with the human hepatocyte RI and can serve as a surrogate measure [15]. We found a positive correlation between ALT and HSA levels (Fig. 1A), indicating that higher levels of liver damage are associated with establishment of higher levels of repopulation of the liver with human hepatocytes. As the human hepatocyte RI obtained in this study using TK-NOG mice is lower than in uPA–SCID mice (Fig 1B), dose escalation of GCV or alternative treatment timing might result in more highly repopulated mice.

We infected humanized TK-NOG mice with hepatitis viruses and compared infection rates and serum viral titers with humanized uPA–SCID mice. HBV inoculation resulted in development of viremia without regard for the human hepatocyte replacement index in both TK-NOG mice and uPA–SCID mice (Fig. 2A). Incidence of HCV viremia was also high in TK-NOG mice regardless of HSA levels, whereas HCV viremia was infrequent in uPA–SCID mice with low HSA levels. These results are consistent with those of Vanwolleghem et al. [20] who showed, using a large number of human hepatocyte chimeric uPA–SCID mice, that an HSA level well above 1 mg/mL is important for successful HCV infection. The reason for the higher infection rate in TK-NOG mice with low human hepatocyte RI in this study is unknown. Although the level of immunodeficiency is higher in TK-NOG mice, it is difficult to conclude that this difference in immunodeficiency alone is responsible for the enhanced HCV infection rate. Although some studies have

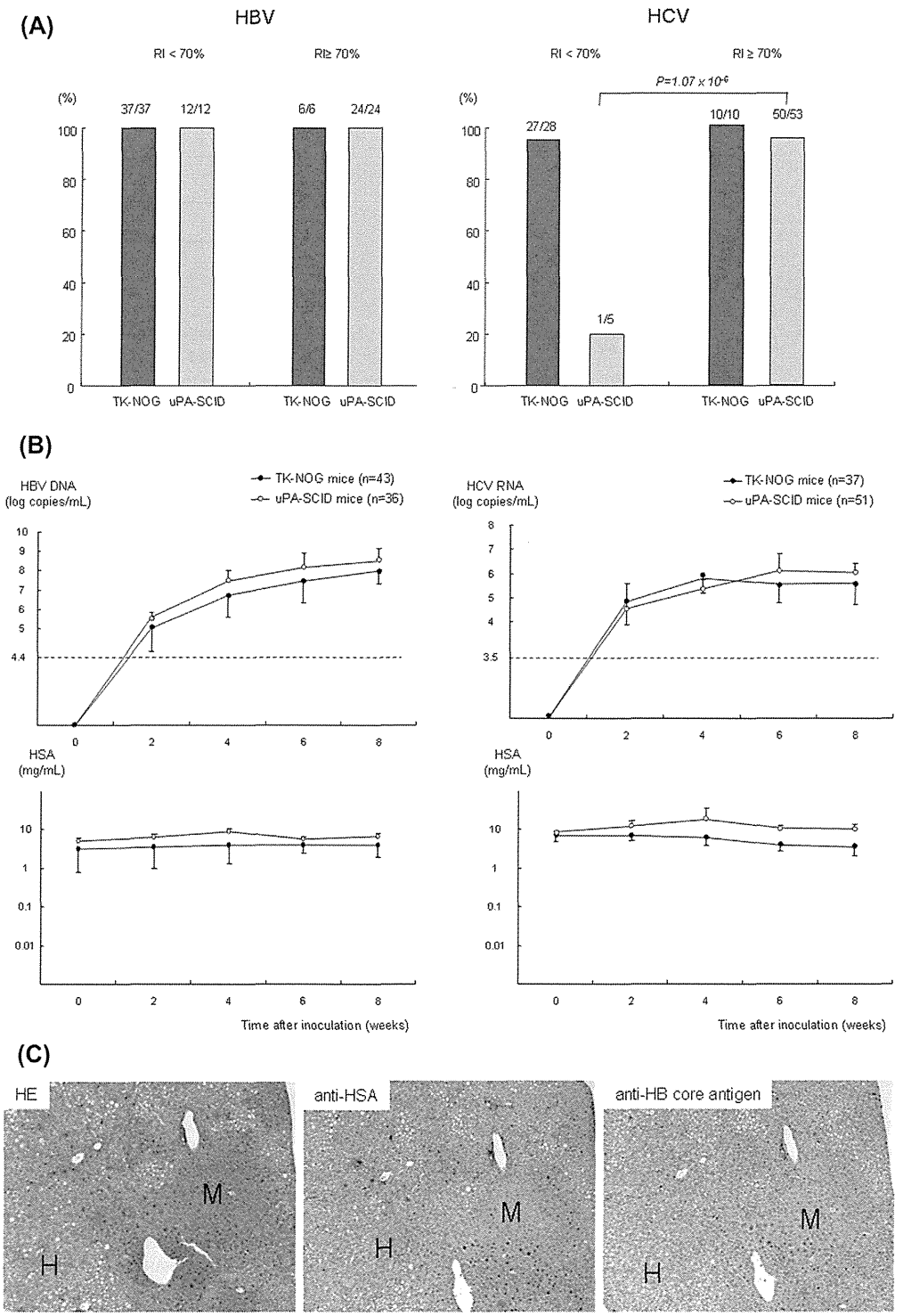

Fig. 2. Hepatitis viruses infection in chimeric mice. (A) Eight weeks after human hepatocyte transplantation, mice with serum HSA level over 1 mg/mL were inoculated with HBV- or HCV-positive human serum samples. Percentages of mice that became positive for HBV DNA (left panel) or HCV RNA (right panel) 8 weeks after inoculation according to human hepatocyte repopulation index (RI) in TK-NOG mice and uPA–SCID mice are shown. 70% of RI corresponds to 5.4 and 6.3 mg/dl of serum HAS in TK-NOG mice and uPA–SCID mice, respectively. (B) Changes in serum titers of HBV DNA (left panel) and HCV RNA (right panel) (upper panels) and HSA levels (lower panels) of TK-NOG mice and uPA–SCID mice. The horizontal dashed lines represent the lower detection limit of HBV DNA and HCV RNA (4.4 and 3.5 log copies/mL, respectively). (C) Histochemical analysis of liver samples obtained from HBV-infected TK-NOG mice. Hematoxylin-eosin staining (HE) and immunohistochemical staining using monoclonal antibodies against HSA and HB core antigen are shown. Regions are shown as human (H) and mouse (M) hepatocytes, respectively (Original magnification 100×).

reported structural differences between wild type and chimeric mice [22,23], the influence of such structural differences on HCV infectivity remains to be determined.

Human hepatocyte transplanted uPA–SCID mice are useful for evaluating antiviral agents [12–14]. In this study, we analyzed the efficacy of antiviral agents such as entecavir, IFN-alpha and

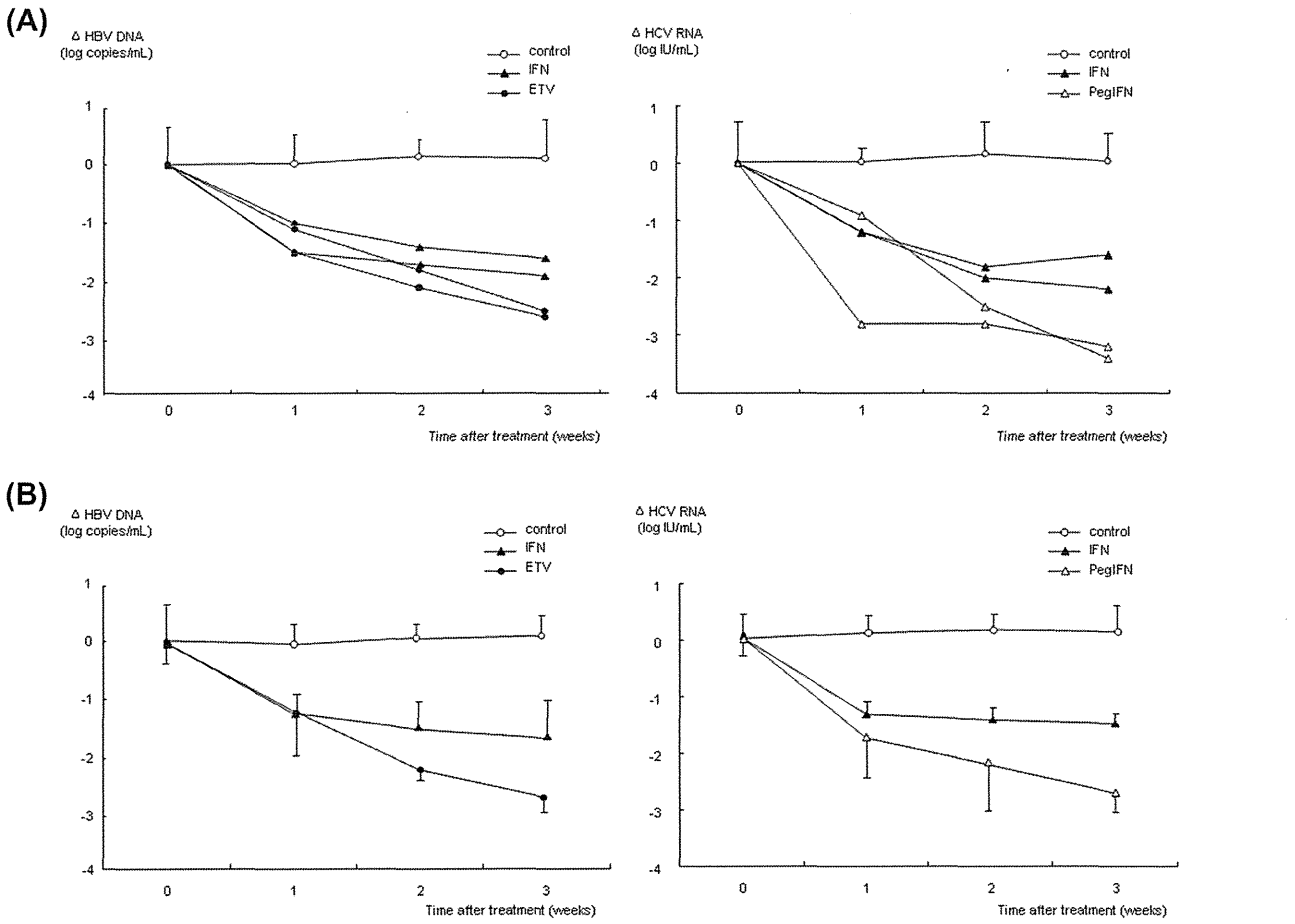

Fig. 3. Reduction of serum viral titers in mice treated with anti-viral agents. (A) HBV- (left panel) or HCV-infected (right panel) TK-NOG mice were treated with entecavir, interferon (IFN)-alpha or PegIFN-alpha-2a. Control: HBV- and HCV-infected mice without antiviral treatment. (B) HBV- (left panel) or HCV-infected (right panel) uPA–SCID mice were treated with entecavir, IFN-alpha or PegIFN-alpha-2a. Data are shown using the mean ± SD ($n = 4$).

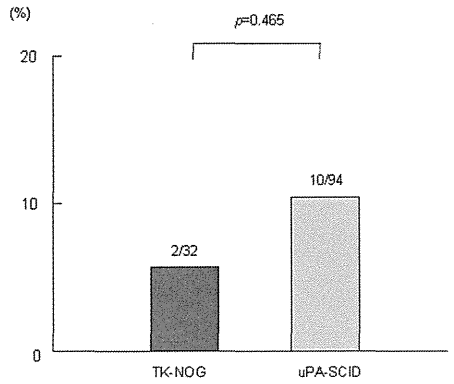

Fig. 4. Frequency of unexpected death within 8 weeks in mice. The numbers of sudden deaths occurring within 8 weeks of viral infection in TK-NOG mice and uPA–SCID mice are shown as bars.

PegIFN-alpha using HBV- and HCV-infected TK-NOG mice and compared them with uPA–SCID mice (Fig. 3). The results showed that both mouse models are equally useful for evaluation of antiviral drugs.

Human hepatocyte chimeric uPA–SCID mice are weak and prone to unexpected death [20], and this limitation appears to apply to TK-NOG mice as well. Incidence of unexpected death in the early stages of viral infection was not significantly different between TK-NOG mice and uPA–SCID mice (Fig. 4). The cause of these unexpected deaths is unknown. Further study is necessary to develop a more robust and easy to manipulate animal model.

In summary, we established a hepatitis virus infection mouse model using the human hepatocyte transplanted TK-NOG mouse. This model is useful for the study of hepatitis virology and evaluation of antiviral agents.

Financial support

This work was supported by Grants-in-Aid for scientific research and development from the Ministry of Health, Labor and Welfare and Ministry of Education Culture Sports Science and Technology, Government of Japan. The funders had no role in study design, data collection and analysis, decision to publish, or preparation of the manuscript. No additional external funding was received for this study.

Acknowledgments

The authors thank Rie Akiyama, and Yoko Matsumoto for their expert technical help. This study was supported in part by a Grant-in-Aid for Scientific Research from the Japanese Ministry of Labor, Health and Welfare.

References

[1] W.C. Maddrey, Hepatitis B: an important public health issue, J. Med. Virol. 61 (2000) 362–366.

[2] Global surveillance and control of hepatitis C, Report of a WHO Consultation organized in collaboration with the Viral Hepatitis Prevention Board, Antwerp, Belgium, J. Viral Hepat. 6 (1999) 35–47.

[3] R.P. Beasley, Hepatitis B virus. The major etiology of hepatocellular carcinoma, Cancer 61 (1988) 1942–1956.

[4] D.F. Mercer, D.E. Schiller, J.F. Elliott, D.N. Douglas, C. Hao, A. Rinfret, W.R. Addison, K.P. Fischer, T.A. Churchill, J.R. Lakey, D.L. Tyrrell, N.M. Kneteman, Hepatitis C virus replication in mice with chimeric human livers, Nat. Med. 7 (2001) 927–933.

[5] C. Tateno, Y. Yoshizane, N. Saito, M. Kataoka, R. Utoh, C. Yamasaki, A. Tachibana, Y. Soeno, K. Asahina, H. Hino, T. Asahara, T. Yokoi, T. Furukawa, K. Yoshizato, Near completely humanized liver in mice shows human-type metabolic responses to drugs, Am. J. Pathol. 165 (2004) 901–912.

[6] H. Azuma, N. Paulk, A. Ranade, C. Dorrell, M. Al-Dhalimy, E. Ellis, S. Strom, M.A. Kay, M. Finegold, M. Grompe, Robust expansion of human hepatocytes in Fah-/-/Rag2-/-/Il2rg-/-mice, Nat. Biotechnol. 25 (2007) 903–910.

[7] K.D. Bissig, T.T. Le, N.B. Woods, I.M. Verma, Repopulation of adult and neonatal mice with human hepatocytes: a chimeric animal model, Proc. Natl. Acad. Sci. USA 104 (2007) 20507–20511.

[8] H. Suemizu, M. Hasegawa, K. Kawai, K. Taniguchi, M. Monnai, M. Wakui, M. Suematsu, M. Ito, G. Peltz, M. Nakamura, Establishment of a humanized model of liver using NOD/Shi-scid IL2Rgnull mice, Biochem. Biophys. Res. Commun. 377 (2008) 248–252.

[9] Y.P. de Jong, C.M. Rice, A. Ploss, New horizons for studying human hepatotropic infections, J. Clin. Invest. 120 (2010) 650–653.

[10] Z. He, H. Zhang, X. Zhang, D. Xie, Y. Chen, K.J. Wangensteen, S.C. Ekker, M. Firpo, C. Liu, D. Xiang, X. Zi, L. Hui, G. Yang, X. Ding, Y. Hu, X. Wang, Liver xeno-repopulation with human hepatocytes in Fah-/-Rag2-/-mice after pharmacological immunosuppression, Am. J. Pathol. 177 (2010) 1311–1319.

[11] K.D. Bissig, S.F. Wieland, P. Tran, M. Isogawa, T.T. Le, F.V. Chisari, I.M. Verma, Human liver chimeric mice provide a model for hepatitis B and C virus infection and treatment, J. Clin. Invest. 120 (2010) 924–930.

[12] M. Tsuge, N. Hiraga, H. Takaishi, C. Noguchi, H. Oga, M. Imamura, S. Takahashi, E. Iwao, Y. Fujimoto, H. Ochi, K. Chayama, C. Tateno, K. Yoshizato, Infection of human hepatocyte chimeric mouse with genetically engineered hepatitis B virus, Hepatology 42 (2005) 1046–1054.

[13] E. Ohara, N. Hiraga, M. Imamura, E. Iwao, N. Kamiya, I. Yamada, T. Kono, M. Onishi, D. Hirata, F. Mitsui, T. Kawaoka, M. Tsuge, S. Takahashi, H. Abe, C.N. Hayes, H. Ochi, C. Tateno, K. Yoshizato, S. Tanaka, K. Chayama, Elimination of hepatitis C virus by short term NS3–4A and NS5B inhibitor combination therapy in human hepatocyte chimeric mice, J. Hepatol. 54 (2011) 872–878.

[14] N. Hiraga, H. Abe, M. Imamura, M. Tsuge, S. Takahashi, C.N. Hayes, H. Ochi, C. Tateno, K. Yoshizato, Y. Nakamura, N. Kamatani, K. Chayama, Impact of viral amino acid substitutions and host interleukin-28b polymorphism on replication and susceptibility to interferon of hepatitis C virus, Hepatology 54 (2011) 764–771.

[15] M. Hasegawa, K. Kawai, T. Mitsui, K. Taniguchi, M. Monnai, M. Wakui, M. Ito, M. Suematsu, G. Peltz, M. Nakamura, H. Suemizu, The reconstituted 'humanized liver' in TK-NOG mice is mature and functional, Biochem. Biophys. Res. Commun. 405 (2011) 405–410.

[16] H. Yamazaki, H. Suemizu, N. Murayama, M. Utoh, N. Shibata, M. Nakamura, F.P. Guengerich, In vivo drug interactions of the teratogen thalidomide with midazolam: heterotropic cooperativity of human cytochrome P450 in humanized TK-NOG mice, Chem. Res. Toxicol. 26 (2013) 486–489.

[17] H. Yamazaki, H. Suemizu, M. Shimizu, S. Igaya, N. Shibata, M. Nakamura, G. Chowdhury, F.P. Guengerich, In vivo formation of dihydroxylated and glutathione conjugate metabolites derived from thalidomide and 5-Hydroxythalidomide in humanized TK-NOG mice, Chem. Res. Toxicol. 25 (2012) 274–276.

[18] Y. Hu, M. Wu, T. Nishimura, M. Zheng, G. Peltz, Human pharmacogenetic analysis in chimeric mice with 'humanized livers', Pharmacogenet. Genomics 23 (2013) 78–83.

[19] N. Hiraga, M. Imamura, M. Tsuge, C. Noguchi, S. Takahashi, E. Iwao, Y. Fujimoto, H. Abe, T. Maekawa, H. Ochi, C. Tateno, K. Yoshizato, A. Sakai, Y. Sakai, M. Honda, S. Kaneko, T. Wakita, K. Chayama, Infection of human hepatocyte chimeric mouse with genetically engineered hepatitis C virus and its susceptibility to interferon, FEBS Lett. 581 (2007) 1983–1987.

[20] T. Vanwolleghem, L. Libbrecht, B.E. Hansen, I. Desombere, T. Roskams, P. Meuleman, G. Leroux-Roels, Factors determining successful engraftment of hepatocytes and susceptibility to hepatitis B and C virus infection in uPA-SCID mice, J. Hepatol. 53 (2010) 468–476.

[21] M. Ito, H. Hiramatsu, K. Kobayashi, K. Suzue, M. Kawahata, K. Hioki, Y. Ueyama, Y. Koyanagi, K. Sugamura, K. Tsuji, T. Heike, T. Nakahata, NOD/SCID/gamma(c) (null) mouse: an excellent recipient mouse model for engraftment of human cells, Blood 100 (2002) 3175–3182.

[22] P. Meuleman, L. Libbrecht, R. De Vos, B. de Hemptinne, K. Gevaert, J. Vandekerckhove, T. Roskams, G. Leroux-Roels, Morphological and biochemical characterization of a human liver in a uPA-SCID mouse chimera, Hepatology 41 (2005) 847–856.

[23] X. Wang, H. Willenbring, Y. Akkari, Y. Torimaru, M. Foster, M. Al-Dhalimy, E. Lagasse, M. Finegold, S. Olson, M. Grompe, Cell fusion is the principal source of bone-marrow-derived hepatocytes, Nature 422 (2003) 897–901.

Cancer Immunol Immunother
DOI 10.1007/s00262-013-1514-7

ORIGINAL ARTICLE

In vivo immunological antitumor effect of OK-432-stimulated dendritic cell transfer after radiofrequency ablation

Hidetoshi Nakagawa · Eishiro Mizukoshi · Noriho Iida · Takeshi Terashima · Masaaki Kitahara · Yohei Marukawa · Kazuya Kitamura · Yasunari Nakamoto · Kazumasa Hiroishi · Michio Imawari · Shuichi Kaneko

Received: 1 June 2013 / Accepted: 17 December 2013

Abstract Radiofrequency ablation therapy (RFA) is a radical treatment for liver cancers and induces tumor antigen-specific immune responses. In the present study, we examined the antitumor effects of focal OK-432-stimulated dendritic cell (DC) transfer combined with RFA and analyzed the functional mechanisms involved using a murine model. C57BL/6 mice were injected subcutaneously with colon cancer cells (MC38) in their bilateral flanks. After the establishment of tumors, the subcutaneous tumor on one flank was treated using RFA, and then OK-432-stimulated DCs were injected locally. The antitumor effect of the treatment was evaluated by measuring the size of the tumor on the opposite flank, and the immunological responses were assessed using tumor-infiltrating lymphocytes, splenocytes and draining lymph nodes. Tumor growth was strongly inhibited in mice that exhibited efficient DC migration after RFA and OK-432-stimulated DC transfer, as compared to mice treated with RFA alone or treatment involving immature DC transfer. We also demonstrated that the antitumor effect of this treatment depended on both CD8-positive and CD4-positive cells. On the basis of our findings, we believe that combination therapy for metastatic liver cancer consisting of OK-432-stimulated DCs in combination with RFA can proceed to clinical trials, and it is anticipated to be markedly superior to RFA single therapy.

Keywords Metastatic liver cancer · MC38 · Immunotherapy · Intratumoral injection · Tumor-infiltrating lymphocyte

Abbreviations

RFA	Radiofrequency ablation
DC	Dendritic cell
HCC	Hepatocellular carcinoma
TAE	Transcatheter hepatic arterial embolization
TLR	Toll-like receptor
GFP	Green fluorescent protein
ELISPOT	Enzyme-linked immunospot
Treg	Regulatory T cell
MDSC	Myeloid-derived suppressor cell
IFN-γ	Interferon-γ

Introduction

Liver is one of the most common organs to which various cancers spread from their site of origin. In some types of cancer, the liver metastasis lesion is a target of surgical treatment. For instance, surgical resection of hepatic metastasis achieves longer median survival in colorectal and breast cancer patients [1, 2]. However, even if the hepatic lesions are surgically treated, the prognosis of the

Electronic supplementary material The online version of this article (doi:10.1007/s00262-013-1514-7) contains supplementary material, which is available to authorized users.

H. Nakagawa · E. Mizukoshi · N. Iida · T. Terashima · M. Kitahara · Y. Marukawa · K. Kitamura · S. Kaneko (✉)
Disease Control and Homeostasis, Graduate School of Medical Sciences, Kanazawa University, 13-1 Takara-machi, Kanazawa, Ishikawa 920-8641, Japan
e-mail: skaneko@m-kanazawa.jp

H. Nakagawa
e-mail: hidetoshi.naka@gmail.com

Y. Nakamoto
Second Department of Internal Medicine, Faculty of Medical Sciences, University of Fukui, Fukui 910-1193, Japan

K. Hiroishi · M. Imawari
Shin-yurigaoka General Hospital, Kawasaki, Kanagawa 215-0026, Japan

Published online: 03 January 2014

patients is not satisfactory. As for colorectal cancers, the recurrence rate is over 50 % after radical resection of metastatic lesions [3]. Moreover, at the time of initial diagnosis, only a few patients meet the criteria for hepatic resection because of unresectability, low hepatic functional reserve or poor performance status [4].

Radiofrequency ablation therapy (RFA) has been developed as a radical and minimally invasive treatment method for metastatic liver cancers. Recently, RFA has been used as an adjunct to hepatic resection or as an alternative method to resection when surgical treatment is not feasible [5]. Additionally, it has been revealed that RFA for metastatic liver cancers generates tumor antigen-specific T-cell responses in man [6, 7]. We have previously reported that RFA could also control distant tumor growth in a murine hepatocellular carcinoma (HCC) model [8].

Dendritic cells (DCs) are potent antigen-presenting cells [9]. Recently, we have established new treatments using local DC injection with transcatheter hepatic arterial embolization (TAE) and have shown that this combination therapy could induce tumor antigen-specific T-cell responses in HCC patients [10].

OK-432 is derived from the Su strain of Group A *Streptococcus pyogenes* by means of treatment with benzylpenicillin and heat [11]. OK-432 can stimulate DCs via Toll-like receptor (TLR) 3, TLR4 and β2 integrin and subsequently induce antigen-specific cytotoxic lymphocytes [12–14].

On the basis of these results, we hypothesized that OK-432-stimulated DC transfer is a promising candidate for an enhancer that can strongly increase the antitumor effect of RFA. We have previously demonstrated in a clinical trial that the local infusion of OK-432-stimulated DC after TAE could prolong recurrence-free survival in HCC patients [15]. However, it remains unknown as to how the transferred DCs work in combination with RFA. In the present study, we examined the antitumor effects of OK-432-stimulated DCs when combined with RFA and analyzed the functional mechanisms involved using a murine subcutaneous colon cancer model.

Materials and methods

Animals

Wild-type 8–12-week-old female C57BL/6 J mice were obtained from Charles River Japan (Yokohama, Japan). Female C57BL/6-Tg (UBC-GFP) 30Scha/J mice were purchased from the Jackson Laboratory (Bar Harbor, ME, USA). All animal experiments were approved and performed in accordance with the Guidelines for the Care and Use of Laboratory Animals of Kanazawa University, which strictly conforms to the Guide for the Care and Use of Laboratory Animals published by the US National Institutes of Health.

Cell lines and bone marrow-derived dendritic cells

A murine colorectal cancer cell line, MC38 and hybridomas, clone GK1.5 and clone 2.43 were cultured in RPMI-1640 containing 10 % fetal bovine serum (Life Technologies, Co., Carlsbad, CA, USA) supplemented with 100 μg/ml streptomycin and 100 units/ml penicillin (Wako Pure Chemical Industries Ltd., Osaka, Japan). Bone marrow-derived dendritic cells (BMDCs) were generated using 20 ng/ml of recombinant granulocyte macrophage colony-stimulating factor (R&D Systems, Minneapolis, MN, USA) as previously described [16]. OK-432 (Picibanil; Chugai Pharmaceutical Co. Ltd., Tokyo, Japan) was loaded into the supernatant from days 6–7 of the BMDC generation period at a concentration of 5 μg/ml.

In vitro evaluation of phagocytic activity by dendritic cells

MC38 cells were labeled with DiD dye (Life Technologies) according to the manufacturer's instructions followed by heat treatment at 80 °C for 90 s. OK-432-stimulated or immature DCs were co-incubated with the treated MC38 cells for 3 h at a ratio of 1:1. After incubation, the cell suspensions were observed using a fluorescence microscope (BZ9000: Keyence, Osaka, Japan) and analyzed by means of FACSCalibur (BD Immuno-Cytometry System, San Jose, CA, USA).

Animal model

Bilateral flanks of C57BL/6 mice were each injected subcutaneously with 1×10^6 MC38 cells. Seven days after injection, after they had grown to 5–6 mm in diameter, the subcutaneous tumors on one flank were treated using RFA, and 1×10^7 immature DCs or 1×10^7 OK-432-stimulated DCs were injected into the treated tumors at 24 h after RFA. After this, the volume of the untreated tumor on the contralateral flank was evaluated over a period of 10 days. Tumor volumes were calculated using the following formula: tumor volume (mm^3) = (longest diameter) × (shortest diameter)^2/2.

Radiofrequency ablation

Mice bearing tumors were anesthetized with an intraperitoneal injection of pentobarbital (Kyoritsu Seiyaku, Tokyo, Japan), and the skin on the tumor was cut. Subsequently, an expandable RFA needle was inserted into the tumor, which was treated using a radiofrequency generator (RITA

500PA; RITA Medical Systems, Inc., Fremont, CA, USA). During the use of this system, the intratumor temperature was maintained at 70–90 °C, and the current was turned off when the tumor exhibited heat denaturation.

Flow cytometry

The DCs were detected by means of staining with anti-CD11c antibodies (Life technologies). The lymphocytes in the draining lymph node were stained with anti-CD4 antibodies, anti-CD8 antibodies, anti-CD11c antibodies and anti-CD69 antibodies (BD Bioscience, San Diego, CA, USA). The splenocytes were stained with anti-CD4 antibodies, anti-CD8 antibodies, CD11c antibodies, anti-NK1.1 antibodies, CD45 antibodies (BD Bioscience), anti-Gr-1 antibodies, and anti-CD11b antibodies and mouse regulatory T-cell staining solution (BioLegend, San Diego, CA, USA). The stained samples were analyzed using FACSAria II (BD Immuno-Cytometry System).

Immunohistochemical assay

The draining lymph nodes and the observed tumors were embedded in Sakura Tissue-Tek optimum cutting temperature compound (Sakura Finetek Japan Co., Ltd., Tokyo, Japan) for frozen sectioning. Tissue sections were fixed at −20 °C in methanol for 10 min. The draining lymph nodes were stained using rabbit anti-GFP antibody (Abcam, Cambridge, UK) that were detected using an EnVision+/HRP kit (Dako, Glostrup, Denmark). The observed tumors were stained with anti-CD4 and anti-CD8a (BD Bioscience), which were detected using the Nichirei Histofine Simple Stain Mouse Max PO (Rat) system (Nichirei Co., Tokyo, Japan) or the Vectastain ABC kit (Vector Laboratory, Inc., Burlingame, CA, USA).

Interferon gamma enzyme-linked immunospot assay

The splenocytes, the tumor-infiltrating lymphocytes (TILs) in the untreated tumors that were isolated by mechanical homogenizations and density gradient centrifugations, and the lymphocytes in the draining lymph nodes were loaded into the interferon gamma enzyme-linked immunospot assay to estimate the tumor-specific immune reactions, as previously described [8, 17]. Briefly, 3×10^5 lymphocytes or 1×10^5 TILs were incubated for 24 h with or without 6×10^5 MC38 lysates, which were prepared through five cycles of rapid freezing in liquid nitrogen, thawing at 55 °C and centrifugation. The number of MC38-specific IFN-γ spots was determined by subtracting the number of spots incubated without MC38 lysates from the number of spots incubated with MC38 lysates. For CD4 or CD8 depletion, we used magnetic CD4 beads or CD8 beads (Miltenyi Biotec, Bergisch Gladbach, Germany).

In vivo CD4/CD8 depletion

For in vivo CD4 or CD8 depletion, B6 mice were injected intraperitoneally with 200 μg of purified monoclonal antibodies specific to CD4 or CD8 at 1 day before and 3 days after RFA treatment; the monoclonal antibodies were prepared from GK1.5 hybridoma and 2.43 hybridoma, respectively [18]. The depletion was confirmed by flow cytometry using peripheral blood lymphocytes stained with anti-CD4 and anti-CD8 antibodies.

Statistical analysis

The data obtained were analyzed statistically using the t test or one-way analysis of variance followed by Tukey's multiple-comparison test. A P value <0.05 was considered as being statistically significant.

Results

Migration efficacy and phagocytic ability of OK-432-stimulated DCs

We employed OK-432 as a modifying agent for DCs, because we have previously shown in clinical studies that OK-432 prolonged recurrence-free survival after combination therapy involving DC injection with TAE for HCC patients [10, 15]. We first confirmed that the OK-432-stimulated murine DCs showed higher expression of maturation markers such as CD40, CD80, CD86, MHC class II and CCR7 (Supplementary Fig. 1), as previously reported [19, 20].

To evaluate their phagocytic abilities, we incubated the immature DCs and the OK-432-stimulated DCs with MC38 tumor cells. Heat-treated MC38 cells were taken up well by both immature DCs and OK-432-stimulated DCs, as compared to nontreated MC38 cells (Fig. 1a–c). In addition, the phagocytic ability of OK-432-stimulated DCs was not inferior to that of immature DCs. These results were consistent with the dextran uptake assay (Supplementary Fig. 2) and our previous data on human monocyte-derived DCs [15]. Since heat-treated MC38 cells were thought to be in a similar condition to those in the MC38 tumor in mice treated with RFA, OK-432-stimulated DCs were expected to effectively phagocytose RFA-treated MC38 tumor cells in vivo.

We next estimated the kinetics of the transferred DCs in mice bearing subcutaneous MC38 tumors treated with RFA. Immature DCs or OK-432-stimulated DCs that were derived from GFP-Tg mice were injected intratumorally

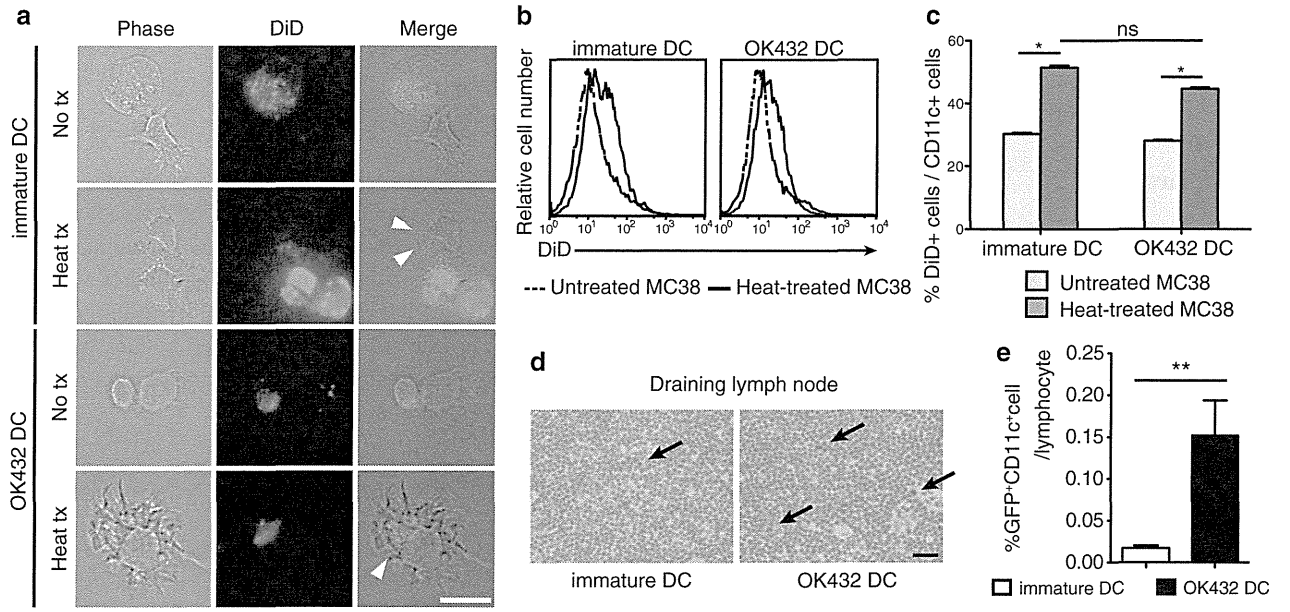

Fig. 1 Effects of OK-432 on murine bone marrow-derived DCs. **a** OK-432-stimulated DCs or immature DCs were co-incubated for 3 h with MC38 cells untreated or treated at 80 °C for 90 s after staining with DiD dye. After incubation, DC and MC38 cells were observed using a fluorescence microscope. *Arrowheads* indicate MC38 derivatives being phagocytosed by DCs. No tx, untreated MC38 cells; heat tx, heat-treated MC38 cells; *bar*, 20 μm. **b**, **c** Co-incubated MC38 cells and DCs were stained with anti-CD11c antibodies and analyzed using flow cytometry. The *histograms* show the DiD fluorescent intensity of the CD11c-positive fractions. The percentages of DiD^+ $CD11c^+$ cells in the $CD11c^+$ cell population are also shown in a *column graph*. The experiments were performed five times, and representative results are shown. Data are presented as the mean ± SE. $^*P < 0.05$. **d** The migration abilities of the DCs after intratumoral transfer were evaluated. The draining lymph nodes were harvested at 3 days after RFA followed by the DC transfer. Frozen sections were prepared and stained with anti-GFP antibodies. *Arrows* indicate the GFP-positive cells in the lymph nodes. *Bar* 20 μm. **e** The draining lymph nodes were also analyzed using flow cytometry after staining with anti-CD11c antibodies. Data were obtained from six mice in each group. Percentages of GFP^+ $CD11c^+$ cell are presented as the mean ± SE. $^{**}P < 0.01$

at 24 h after RFA treatment, and the subcutaneous tumors and the lymph nodes were harvested at 3 days after RFA. According to the immunohistochemical study involving the detection of GFP, the inguinal lymph node on the RFA-treated flank was thought to be the draining lymph node (Supplementary Fig. 3). Additionally, the number of transferred DCs in the draining lymph nodes was significantly higher in the mice treated with the OK-432-stimulated DCs than in those treated with the immature DCs (Fig. 1d, e). Our experimental results attested to the fact that the OK-432-stimulated DCs had both sufficient phagocytic ability and higher migration efficacy.

Effect of RFA in combination with the injection of OK-432-stimulated DCs on tumor growth

OK-432-stimulated DCs were used in combination therapy with RFA in this murine model (Fig. 2a). Namely, BMDCs stimulated with OK-432 were injected into RFA-treated tumor at 24 h after RFA treatment. We compared four groups of tumor-bearing mice as follows: (1) no treatment; (2) RFA only; (3) RFA with the injection of immature DCs; and (4) RFA with the injection of OK-432-stimulated DCs. Tumor volumes were measured for 10 days after treatment/no treatment. On the day after RFA, the treated tumors were covered with scars, started to shrink and had disappeared macroscopically at 4 days after RFA in all of the groups. This indicated that RFA treatment was highly effective for focal lesions. The injected DCs were detected in the treated tumors (Supplementary Fig. 3). With regard to the untreated tumors, as we previously reported, the group treated with RFA only showed an antitumor effect against distant tumors. The injection of immature DCs combined with RFA did not show any additional enhancement of the antitumor effect. On the other hand, the volumes of the untreated tumors in the group that underwent RFA combined with the injection of OK-432-stimulated DCs were strongly suppressed ($P < 0.001$) relative to other groups (Fig. 2b).

Recruitment of antigen-specific lymphocyte fractions in both splenocytes and tumor by injected OK-432-stimulated DCs

Ten days after RFA, the tumors and the spleens were harvested and analyzed using immunohistochemical staining.

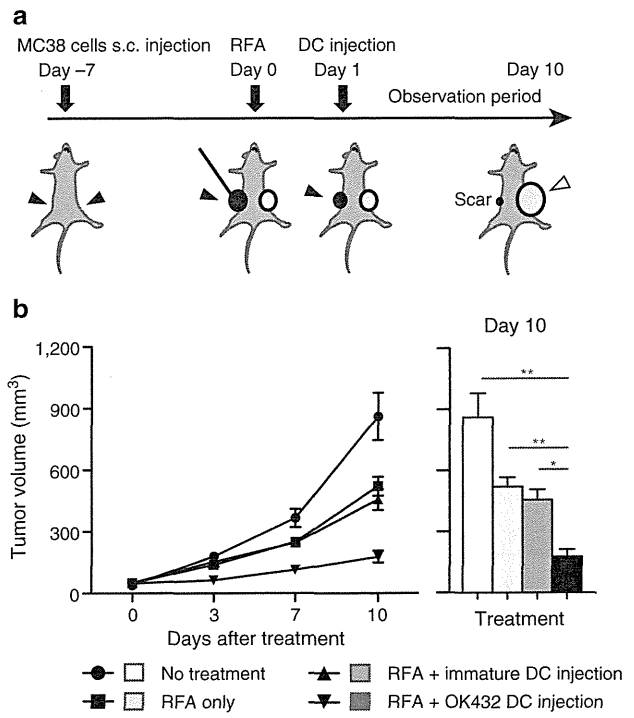

Fig. 2 Impact of injection of OK-432-stimulated DCs into murine MC38 subcutaneous tumors. **a** RFA was administered to a tumor on one flank followed by injection of 1×10^7 DCs into the treated tumor. The untreated tumor on the opposite flank was observed for 10 days. The *solid arrowheads* indicate the treatment intervention sites, and the *open arrowhead* indicates the observed untreated tumor. **b** The tumor volumes were compared among the four groups as follows: (1) no treatment; (2) RFA only; (3) RFA in combination with immature DC injection; and (4) RFA in combination with OK-432-stimulated DC injection. $n = 8$ mice per group. The data are presented as the mean ± SE. $^*P < 0.05$; $^{**}P < 0.001$

We examined the number of tumor-infiltrating CD4-positive or CD8-positive cells in the tumors by means of immunohistochemistry. The infiltration of these cells into the untreated tumors was found to be promoted by RFA. The injection of OK-432-stimulated DCs after RFA induced the additional recruitment of CD8-positive cells into the untreated tumors (Fig. 3a, b). CD11c-, CD11b- and NK1.1-positive cells were very marginal and showed no differences in number among the four groups (data not shown).

Systemically, in terms of analyzing splenocytes with flow cytometry, the number of CD4-positive and CD8-positive cells increased in the group treated with RFA in combination with OK-432-stimulated DCs. On the other hand, the CD11c and NK1.1 fractions, which were considered as DCs and NK cells, respectively, presented no difference among the four groups (Fig. 3c). In addition, we examined the effect of the injection of OK-432-stimulated DCs after RFA on inhibitory blood cells such as regulatory T cells (Tregs) and myeloid-derived suppressor cells (MDSCs) (Fig. 3c). Among CD4-positive cells, significantly fewer Tregs were detected in the group treated with RFA in combination with OK-432-stimulated DCs than in the group treated with RFA in combination with immature DCs. In the analysis of MDSCs, their rates of occurrence were not affected by treatment with either RFA alone or RFA in combination with DCs. Taking these results together, we concluded that treatment with RFA combined with OK-432-stimulated DCs enhanced the number of CD4- or CD8-positive T cells and reduced the Treg/CD4 ratio, but did not influence MDSC numbers.

Furthermore, we examined the number of tumor-specific IFN-γ-producing cells at 10 days after RFA using the ELISPOT assay. The number of IFN-γ-producing cells among splenocytes and TILs showed the same trend as the level of tumor growth control among the four groups (Fig. 3d); the group treated with RFA in combination with injected OK-432 DCs showed the most abundant specific spots. These results suggested that the augmented antitumor effects of RFA combined with OK-432-stimulated DCs depended in large part on tumor-specific immune responses by CD4 cells or CD8 cells.

Evaluation of tumor-specific immune responses in the draining lymph node after OK-432-stimulated DC transfer

CD4 T cells and CD8 T cells are now thought to have an important antitumor effect as a result of the OK-432-stimulated DC transfer. To elucidate the priming of the antigen-specific immune response, we analyzed the draining lymph nodes at 3 days after RFA focusing on CD4-positive or CD8-positive cells. CD69, the early activation marker, on CD4-positive and CD8-positive cells was examined and compared between the immature DC transfer group and the OK-432-stimulated DC transfer group. It was found that CD69 expression on both CD4-positive and CD8-positive cells was elevated in the OK-432-stimulated DC transfer group (Fig. 4a, b). The activations were also demonstrated to be tumor-specific using the IFN-γ ELISPOT assay in which each of CD4-negative and CD8-negative fractions was applied to the assay and both showed tumor-specific IFN-γ secretions (Fig. 4c).

Evaluation of the relationship between CD4-positive and CD8-positive cells and the antitumor effects of RFA and OK-432-stimulated DC transfer

We have demonstrated that combination therapy involving RFA and OK-432-stimulated DC transfer might generate enhanced antitumor effects via tumor-specific CD4-positive and CD8-positive cells. To obtain further evidence, we carried out in vivo CD4 or CD8 depletion studies in mice. Initially, we confirmed CD4 or CD8 depletion in the control in vivo study (Supplementary Fig. 4). The

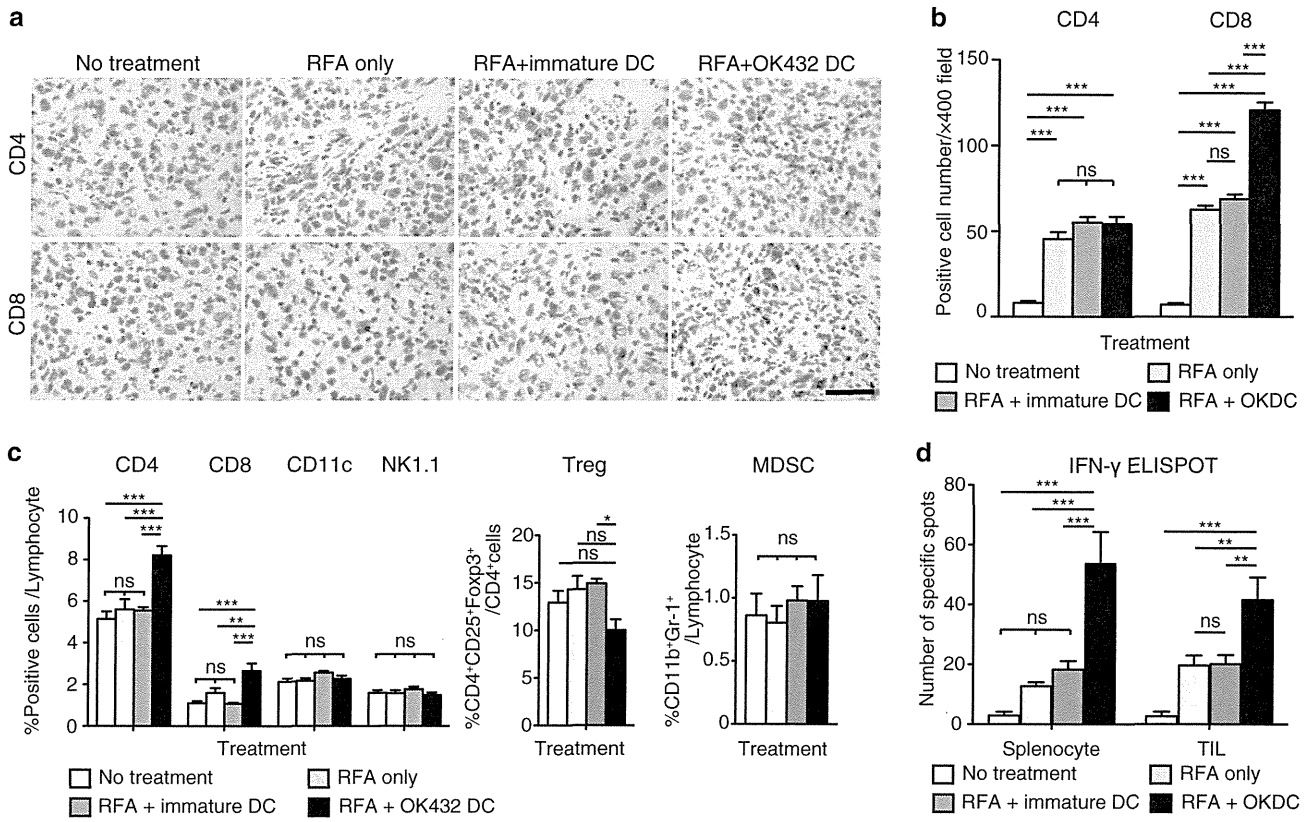

Fig. 3 Analysis of the tumor-infiltrating lymphocytes and the splenocytes after combination therapy with RFA and DC injection. **a** CD4-positive and CD8-positive cells in the observed untreated tumors were detected using immunohistochemistry at 10 days after RFA. The *black bar* represents 50 μm. **b** The number of positive cells was counted using a microscope. This was achieved by counting the number of cells in six randomly chosen tumor areas at 400-fold magnification. Three mice were used in each group. The data are presented as the mean ± SE. *** $P < 0.001$; *ns* not significant. **c** Ten days after RFA, splenocytes were stained with anti-CD4, anti-CD8, anti-NK1.1 and anti-CD11c antibodies and analyzed using flow cytometry. Regulatory T cells (Tregs) defined as $CD4^+CD25^+Foxp3^+$ cells and myeloid-derived suppressor cells (MDSCs) defined as $CD11b^+Gr\text{-}1^+$ cells were counted and compared among the four groups. Six mice were analyzed in each group. The data are presented as the mean ± SE. *$P < 0.05$; **$P < 0.01$; ***$P < 0.001$; *ns* not significant. **d** Immune responses by the splenocytes and the tumor-infiltrating lymphocytes (TILs) were examined by means of the IFN-γ enzyme-linked immunospot (ELISPOT) assay using MC38 lysate. In the assay for TILs, 1×10^5 TILs were mixed with 2×10^5 splenocytes from B6 mice and applied to the well. Six mice were analyzed in each group. The data are presented as the mean ± SE. **$P < 0.01$; ***$P < 0.001$; *ns* not significant

CD4-positive and CD8-positive fractions in the peripheral blood were greatly depleted at 7 days after injection of the antibodies. The experimental schedule was determined as follows. The depletion antibodies were injected at 1 day before and 3 days after RFA, and the tumors that were not treated with RFA were observed for 10 days. In addition, the draining lymph nodes were harvested at 3 days after RFA and analyzed (Supplementary Fig. 5). The antitumor effects of RFA treatment and the augmented effects from OK-432-stimulated DCs were cancelled out by depletion of both CD4 and CD8 cells (Fig. 5a). In the CD4 depletion study, there was no priming of the antitumor effect in the draining lymph nodes (Fig. 5b; Supplementary Fig. 6). On the other hand, in the CD8 depletion study CD4 cells were activated with tumor specificities in the draining lymph node in both groups, and the activation was stronger in the OK-432-stimulated DC transfer group (Fig. 5b; Supplementary Fig. 6). Tumor-specific reactions were also demonstrated in the splenocytes and the TILs at 10 days after RFA. There was a tendency for OK-432 DC transfer treatment to result in the recruitment of increased numbers of tumor-specific lymphocytes into the tumor on the opposite flank ($P = 0.184$; Fig. 5c). These results indicated that the tumor-specific activation of CD8 cells was necessary for the antitumor effect and was completely dependent on help from the CD4 cells.

Discussion

In the past decade, cytotoxic agents and molecular-targeted therapies have been developed, and the treatment outcomes

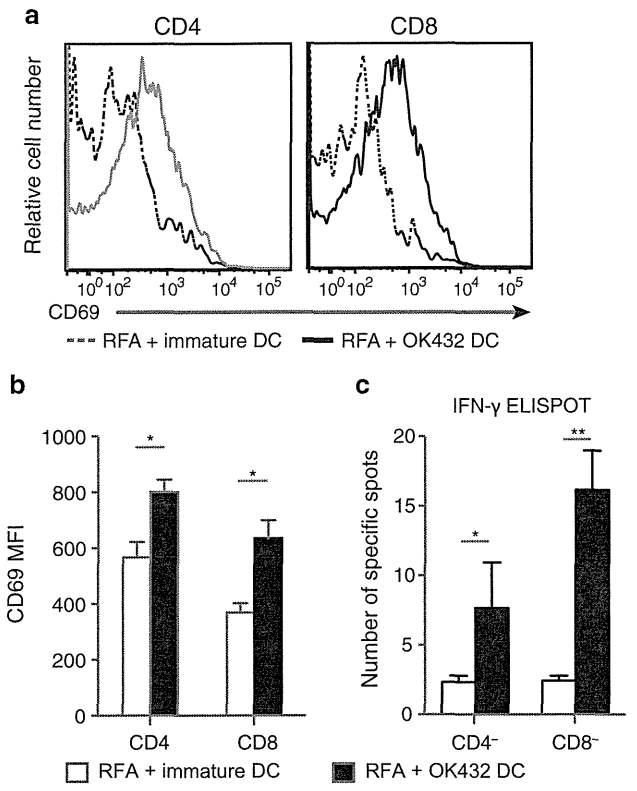

Fig. 4 Antigen-specific activation of both CD4-positive and CD8-positive cells in the draining lymph node. **a** Three days after RFA followed by DC transfer, the draining lymph node was harvested and analyzed by staining with anti-CD4 antibodies, anti-CD8 antibodies and anti-CD69 antibodies. The fluorescence intensities of CD69 in the CD4-positive and CD8-positive fractions are compared between the OK-432-stimulated DC transfer group and the immature DC transfer group. The data were obtained from six mice in each group. The *histograms* show the representative data. **b** The mean fluorescent intensities are also presented as the mean ± SE. $*P < 0.05$. **c** The antigen specificities of the T-cell activations were confirmed by means of the IFN-γ ELISPOT assay using MC38 lysate. After CD4 or CD8 depletion using CD4 and CD8 magnetic beads, the lymphocytes from the draining lymph nodes were submitted to IFN-γ ELISPOT assay. Data were obtained from six mice in each group. $*P < 0.05$; $**P < 0.01$

for various cancers have improved. However, few patients with advanced cancers have been completely cured, and thus, new strategies for anticancer therapy are required. Immunotherapy is considered to have the potential to effectively treat such advanced cancers, and many different approaches have been explored. For the utilization of the adoptive immune response in a cancer therapy, DCs are a key constituent of the immune system. This is because of their natural potential to present tumor-associated antigens to $CD4^+$ and $CD8^+$ lymphocytes and also to control both immune tolerance and immunity [21]. Thus, DCs are considered as an important target for cancer immunotherapy. Many trials and studies have been carried out regarding immunotherapy for cancer using DCs, some of which have been reported to have pronounced effects [22–25]. In recent studies, it has been revealed that RFA treatment induces tumor-specific T-cell responses, which is known as the abscopal effect; this has been mainly reported in radiotherapy studies and is augmented with combined immunotherapies [26, 27]. Brok et al. [28] have previously reported on the vaccination effects of combination therapy involving RFA and CTLA-4 antibody.

To our knowledge, this is the first study that has demonstrated using a murine metastatic cancer model that RFA in combination with focal DC injection could enhance the antitumor effects of RFA alone. Our results showed that immature DCs made no additional immunological contribution to RFA. In the analysis of draining lymph nodes, few transferred DCs were detected after the injection of immature DCs. It appeared that immature DCs did not act as sentinels in the adoptive immune system, partially because they exhibited low expression of CCR7 (the main molecule that promotes DC migration [29]), even though elevation of CCR7 expression using OK-432 was very modest in our study. There is another possibility immature DCs are easily lysed and excluded by the host immune system [30]. On the other hand, mature DCs can escape cell lysis [31].

Utilization of OK-432-stimulated DCs improved the number of migrating transferred DCs in the present study. These DCs, which could act as sentinels for immunity, induced expansion in the number of tumor-specific lymphocytes in the draining lymph nodes, in the splenocytes and in the distant nontreated tumors, without systemic expansion of inhibitory cells such as Tregs or MDSCs. We also demonstrated that these augmented antitumor effects after OK-432-stimulated DC transfer were primed in the draining lymph nodes with tumor-specific activations of CD4-positive and CD8-positive cells; it was proved that without CD4-positive or CD8-positive cells, both the antitumor effect by RFA and the additional effect of the injection of OK-432-stimulated DCs disappeared completely. In addition, the in vivo CD4 depletion study revealed that tumor-specific activations of CD8-positive cells were not seen in the draining lymph nodes in both groups after the injection of immature DCs and OK-432-stimulated DC injection; in other words, tumor-specific CD8 activation depended on CD4-positive cells entirely. In the CD8 depletion study, on the other hand, we found that tumor-specific CD4-positive cells appeared in the draining lymph nodes, the splenocyte population and the untreated tumor on the opposite flank, and these lymphocytes were considered to be CD4-positive cells. In the tumor-infiltrating lymphocytes, there was a tendency for more tumor-specific CD4-positive cells to be recruited after treatment involving OK-432-stimulated DC transfer. Many researchers have demonstrated the contribution of CD4 cells to cytotoxicity

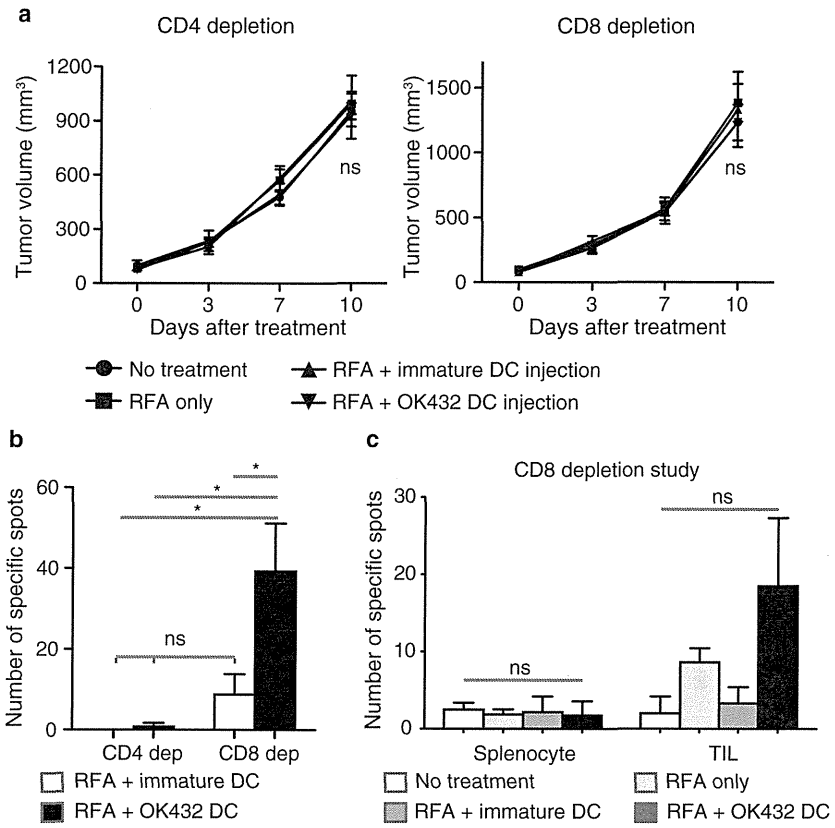

Fig. 5 The augmented antitumor effects depended on both CD4-positive and CD8-positive cells. **a** For in vivo CD4 or CD8 depletion, monoclonal antibodies specific to CD4 (GK1.5) or CD8 (2.43), respectively, were injected intraperitoneally at 1 day before and 3 days after RFA. Tumor volumes were compared among the four groups for 10 days after RFA. In each experiment, data were obtained from four mice per group and are presented as the mean ± SE. *ns* not significant. **b** The draining lymph nodes were harvested at 3 days after RFA and analyzed for their tumor specificities using the IFN-γ ELISPOT assay. Two mice were used in each group. Data are shown as the mean ± SE. $*P < 0.005$; *ns* not significant. **c** In the CD8 depletion study, splenocytes and tumor-infiltrating lymphocytes (TILs) were evaluated for their tumor specificities using the IFN-γ ELISPOT assay as described in Fig. 3. Four mice were used in each group. Data are shown as the mean ± SE. *ns* not significant

[32, 33]. However, in our experimental models, tumor-specific CD4-positive cells were not observed to contribute to the antitumor effect. Summarizing the above, in our study, the CD4-positive cells were required for the priming of the immune responses, and the CD8-positive cells acted as the effector cells after help from the CD4-positive cells.

In conclusion, we consider on the basis of our preclinical findings regarding combination therapy involving OK-432-stimulated DCs with RFA for the treatment of metastatic liver cancer that clinical trials can now proceed. It is anticipated that this combination therapy will be markedly superior to RFA single therapy.

Acknowledgments The authors thank Ms. Fushimi and Ms. Baba for technical support. This study was supported by research grants from the Ministry of Education, Culture, Sports, Science and Technology of Japan.

Conflict of interest The authors received financial support for this study from Chugai Pharmaceutical Co., Ltd.

References

1. Ruiterkamp J, Ernst MF, de Munck L, van der Heiden, van der Loo M, Bastiaannet E, van de Poll-Franse LV, Bosscha K, Tjan-Heijnen VC, Voogd AC (2011) Improved survival of patients with primary distant metastatic breast cancer in the period of 1995–2008. A nationwide population-based study in the Netherlands. Breast Cancer Res Treat 128(2):495–503. doi:10.1007/s10549-011-1349-x
2. Simmonds PC, Primrose JN, Colquitt JL, Garden OJ, Poston GJ, Rees M (2006) Surgical resection of hepatic metastases from colorectal cancer: a systematic review of published studies. Br J Cancer 94(7):982–999. doi:10.1038/sj.bjc.6603033
3. Nordlinger B, Guiguet M, Vaillant JC, Balladur P, Boudjema K, Bachellier P, Jaeck D (1996) Surgical resection of colorectal carcinoma metastases to the liver. A prognostic scoring system to improve case selection, based on 1568 patients. Association Francaise de Chirurgie. Cancer 77(7):1254–1262
4. Bentrem DJ, Dematteo RP, Blumgart LH (2005) Surgical therapy for metastatic disease to the liver. Annu Rev Med 56:139–156. doi:10.1146/annurev.med.56.082103.104630
5. Meyers MO, Sasson AR, Sigurdson ER (2003) Locoregional strategies for colorectal hepatic metastases. Clin Colorectal Cancer 3(1):34–44. doi:10.3816/CCC.2003.n.010

6. Napoletano C, Taurino F, Biffoni M, De Majo A, Coscarella G, Bellati F, Rahimi H, Pauselli S, Pellicciotta I, Burchell JM, Gaspari LA, Ercoli L, Rossi P, Rughetti A (2008) RFA strongly modulates the immune system and anti-tumor immune responses in metastatic liver patients. Int J Oncol 32(2):481–490
7. Nobuoka D, Motomura Y, Shirakawa H, Yoshikawa T, Kuronuma T, Takahashi M, Nakachi K, Ishii H, Furuse J, Gotohda N, Takahashi S, Nakagohri T, Konishi M, Kinoshita T, Komori H, Baba H, Fujiwara T, Nakatsura T (2012) Radiofrequency ablation for hepatocellular carcinoma induces glypican-3 peptide-specific cytotoxic T lymphocytes. Int J Oncol 40(1):63–70. doi:10.3892/ijo.2011.1202
8. Iida N, Nakamoto Y, Baba T, Nakagawa H, Mizukoshi E, Naito M, Mukaida N, Kaneko S (2010) Antitumor effect after radiofrequency ablation of murine hepatoma is augmented by an active variant of CC Chemokine ligand 3/macrophage inflammatory protein-1 alpha. Cancer Res 70(16):6556–6565. doi:10.1158/0008-5472.CAN-10-0096
9. Banchereau J, Briere F, Caux C, Davoust J, Lebecque S, Liu YJ, Pulendran B, Palucka K (2000) Immunobiology of dendritic cells. Annu Rev Immunol 18:767–811. doi:10.1146/annurev.immunol.18.1.767
10. Nakamoto Y, Mizukoshi E, Tsuji H, Sakai Y, Kitahara M, Arai K, Yamashita T, Yokoyama K, Mukaida N, Matsushima K, Matsui O, Kaneko S (2007) Combined therapy of transcatheter hepatic arterial embolization with intratumoral dendritic cell infusion for hepatocellular carcinoma: clinical safety. Clin Exp Immunol 147(2):296–305. doi:10.1111/j.1365-2249.2006.03290.x
11. Ryoma Y, Moriya Y, Okamoto M, Kanaya I, Saito M, Sato M (2004) Biological effect of OK-432 (picibanil) and possible application to dendritic cell therapy. Anticancer Res 24(5C):3295–3301
12. Nakahara S, Tsunoda T, Baba T, Asabe S, Tahara H (2003) Dendritic cells stimulated with a bacterial product, OK-432, efficiently induce cytotoxic T lymphocytes specific to tumor rejection peptide. Cancer Res 63(14):4112–4118
13. Okamoto M, Oshikawa T, Tano T, Ahmed SU, Kan S, Sasai A, Akashi S, Miyake K, Moriya Y, Ryoma Y, Saito M, Sato M (2006) Mechanism of anticancer host response induced by OK-432, a streptococcal preparation, mediated by phagocytosis and Toll-like receptor 4 signaling. J Immuno ther 29(1):78–86
14. Hovden AO, Karlsen M, Jonsson R, Appel S (2012) The bacterial preparation OK432 induces IL-12p70 secretion in human dendritic cells in a TLR3 dependent manner. PLoS ONE 7(2):e31217. doi:10.1371/journal.pone.0031217
15. Nakamoto Y, Mizukoshi E, Kitahara M, Arihara F, Sakai Y, Kakinoki K, Fujita Y, Marukawa Y, Arai K, Yamashita T, Mukaida N, Matsushima K, Matsui O, Kaneko S (2011) Prolonged recurrence-free survival following OK432-stimulated dendritic cell transfer into hepatocellular carcinoma during transarterial embolization. Clin Exp Immunol 163(2):165–177. doi:10.1111/j.1365-2249.2010.04246.x
16. Inaba K, Inaba M, Romani N, Aya H, Deguchi M, Ikehara S, Muramatsu S, Steinman RM (1992) Generation of large numbers of dendritic cells from mouse bone marrow cultures supplemented with granulocyte/macrophage colony-stimulating factor. J Exp Med 176(6):1693–1702
17. Mizukoshi E, Nakamoto Y, Marukawa Y, Arai K, Yamashita T, Tsuji H, Kuzushima K, Takiguchi M, Kaneko S (2006) Cytotoxic T cell responses to human telomerase reverse transcriptase in patients with hepatocellular carcinoma. Hepatology 43(6):1284–1294. doi:10.1002/hep.21203
18. Nakamoto Y, Suda T, Momoi T, Kaneko S (2004) Different procarcinogenic potentials of lymphocyte subsets in a transgenic mouse model of chronic hepatitis B. Cancer Res 64(9):3326–3333
19. Okamoto M, Furuichi S, Nishioka Y, Oshikawa T, Tano T, Ahmed SU, Takeda K, Akira S, Ryoma Y, Moriya Y, Saito M, Sone S, Sato M (2004) Expression of toll-like receptor 4 on dendritic cells is significant for anticancer effect of dendritic cell-based immunotherapy in combination with an active component of OK-432, a streptococcal preparation. Cancer Res 64(15):5461–5470. doi:10.1158/0008-5472.CAN-03-4005
20. Hill KS, Errington F, Steele LP, Merrick A, Morgan R, Selby PJ, Georgopoulos NT, O'Donnell DM, Melcher AA (2008) OK432-activated human dendritic cells kill tumor cells via CD40/CD40 ligand interactions. J Immunol 181(5):3108–3115
21. Banchereau J, Steinman RM (1998) Dendritic cells and the control of immunity. Nature 392(6673):245–252. doi:10.1038/32588
22. Timmerman JM, Czerwinski DK, Davis TA, Hsu FJ, Benike C, Hao ZM, Taidi B, Rajapaksa R, Caspar CB, Okada CY, van Beckhoven A, Liles TM, Engleman EG, Levy R (2002) Idiotype-pulsed dendritic cell vaccination for B-cell lymphoma: clinical and immune responses in 35 patients. Blood 99(5):1517–1526
23. Banchereau J, Palucka AK, Dhodapkar M, Burkeholder S, Taquet N, Rolland A, Taquet S, Coquery S, Wittkowski KM, Bhardwaj N, Pineiro L, Steinman R, Fay J (2001) Immune and clinical responses in patients with metastatic melanoma to CD34(+) progenitor-derived dendritic cell vaccine. Cancer Res 61(17):6451–6458
24. Okada H, Kalinski P, Ueda R, Hoji A, Kohanbash G, Donegan TE, Mintz AH, Engh JA, Bartlett DL, Brown CK, Zeh H, Holtzman MP, Reinhart TA, Whiteside TL, Butterfield LH, Hamilton RL, Potter DM, Pollack IF, Salazar AM, Lieberman FS (2011) Induction of CD8 + T-cell responses against novel glioma-associated antigen peptides and clinical activity by vaccinations with {alpha}-type 1 polarized dendritic cells and polyinosinic-polycytidylic acid stabilized by lysine and carboxymethylcellulose in patients with recurrent malignant glioma. J Clin Oncol 29(3):330–336. doi:10.1200/JCO.2010.30.7744
25. Suso EM, Dueland S, Rasmussen AM, Vetrhus T, Aamdal S, Kvalheim G, Gaudernack G (2011) hTERT mRNA dendritic cell vaccination: complete response in a pancreatic cancer patient associated with response against several hTERT epitopes. Cancer Immunol Immunother 60(6):809–818. doi:10.1007/s00262-011-0991-9
26. Frey B, Weiss EM, Rubner Y, Wunderlich R, Ott OJ, Sauer R, Fietkau R, Gaipl US (2012) Old and new facts about hyperthermia-induced modulations of the immune system. Int J Hyperthermia 28(6):528–542. doi:10.3109/02656736.2012.677933
27. Rubner Y, Wunderlich R, Ruhle PF, Kulzer L, Werthmoller N, Frey B, Weiss EM, Keilholz L, Fietkau R, Gaipl US (2012) How does ionizing irradiation contribute to the induction of anti-tumor immunity? Front Oncol 2:75. doi:10.3389/fonc.2012.00075
28. den Brok MH, Sutmuller RP, van der Voort R, Bennink EJ, Figdor CG, Ruers TJ, Adema GJ (2004) In situ tumor ablation creates an antigen source for the generation of antitumor immunity. Cancer Res 64(11):4024–4029. doi:10.1158/0008-5472.CAN-03-3949
29. Forster R, Schubel A, Breitfeld D, Kremmer E, Renner-Muller I, Wolf E, Lipp M (1999) CCR7 coordinates the primary immune response by establishing functional microenvironments in secondary lymphoid organs. Cell 99(1):23–33
30. Ferlazzo G, Tsang ML, Moretta L, Melioli G, Steinman RM, Munz C (2002) Human dendritic cells activate resting natural killer (NK) cells and are recognized via the NKp30 receptor by activated NK cells. J Exp Med 195(3):343–351
31. Morandi B, Mortara L, Chiossone L, Accolla RS, Mingari MC, Moretta L, Moretta A, Ferlazzo G (2012) Dendritic cell editing by activated natural killer cells results in a more protective cancer-specific immune response. PLoS ONE 7(6):e39170. doi:10.1371/journal.pone.0039170.

32. Ab BK, Kiessling R, Van Embden JD, Thole JE, Kumararatne DS, Pisa P, Wondimu A, Ottenhoff TH (1990) Induction of antigen-specific CD4+ HLA-DR-restricted cytotoxic T lymphocytes as well as nonspecific nonrestricted killer cells by the recombinant mycobacterial 65-kDa heat-shock protein. Eur J Immunol 20(2):369–377. doi:10.1002/eji.1830200221

33. Bourgault I, Gomez A, Gomard E, Picard F, Levy JP (1989) A virus-specific CD4+ cell-mediated cytolytic activity revealed by CD8+ cell elimination regularly develops in uncloned human antiviral cell lines. J Immunol 142(1):252–256

Coordinated Changes in DNA Methylation in Antigen-Specific Memory CD4 T Cells

Shin-ichi Hashimoto,*,†,‡ Katsumi Ogoshi,* Atsushi Sasaki,† Jun Abe,* Wei Qu,† Yoichiro Nakatani,† Budrul Ahsan,§ Kenshiro Oshima,† Francis H. W. Shand,* Akio Ametani,* Yutaka Suzuki,¶ Shuichi Kaneko,‖ Takashi Wada,‡ Masahira Hattori,† Sumio Sugano,¶ Shinichi Morishita,† and Kouji Matsushima*

Memory CD4$^+$ T cells are central regulators of both humoral and cellular immune responses. T cell differentiation results in specific changes in chromatin structure and DNA methylation of cytokine genes. Although the methylation status of a limited number of gene loci in T cells has been examined, the genome-wide DNA methylation status of memory CD4$^+$ T cells remains unexplored. To further elucidate the molecular signature of memory T cells, we conducted methylome and transcriptome analyses of memory CD4$^+$ T cells generated using T cells from TCR-transgenic mice. The resulting genome-wide DNA methylation profile revealed 1144 differentially methylated regions (DMRs) across the murine genome during the process of T cell differentiation, 552 of which were associated with gene loci. Interestingly, the majority of these DMRs were located in introns. These DMRs included genes such as CXCR6, Tbox21, Chsy1, and Cish, which are associated with cytokine production, homing to bone marrow, and immune responses. Methylation changes in memory T cells exposed to specific Ag appeared to regulate enhancer activity rather than promoter activity of immunologically relevant genes. In addition, methylation profiles differed between memory T cell subsets, demonstrating a link between T cell methylation status and T cell differentiation. By comparing DMRs between naive and Ag-specific memory T cells, this study provides new insights into the functional status of memory T cells. ***The Journal of Immunology*****, 2013, 190: 4076–4091.**

CD4$^+$ T cells are central regulators of both humoral and cellular immune responses. Activation of naive CD4$^+$ T cells by Ag induces cell proliferation, resulting in the formation of a large number of effector cells and, subsequently, a limited number of memory cells. Memory CD4$^+$ T cell populations are maintained by cytokine survival signals and homeostatic proliferation, such that they are able to respond rapidly to subsequent exposure to the same Ag (1, 2). Recently, it was reported that the first exposure of a naive T cell to Ag and cytokine signals results in specific changes in the cell's chromatin structure and in DNA methylation of the cell's cytokine genes (3–5).

Chromatin modifications are known to impose epigenetic controls on gene expression without changing DNA sequence (6). These modifications determine the level of cell type–specific gene transcription by modulating the accessibility of genes to transcription factors and the basal transcription apparatus. It is well known that epigenetic regulation is linked to gene repression of oncogenes and development-related genes (6, 7). Genes that are active (open) in a particular tissue or cell type have increased acetylation and methylation of their histones (e.g., H3K4 methylation), whereas genes that are inactive (closed) are characterized by highly condensed chromatin and decreased acetylation and methylation of their histones (e.g., H3K9 and H3K27 methylation). In addition, DNA methyltransferases establish and maintain the pattern of genomic DNA methylation of cytosines in CpG dinucleotides. DNA methylation status is generally considered to correlate inversely with transcriptional activity, with transcriptionally silent genes being highly methylated and transcriptionally active regions being relatively unmethylated (8, 9). DNA methylation is also associated with epigenetic gene regulation during embryogenesis, genomic imprinting, and X-chromosome inactivation (10, 11).

In the immune system, a lack of methylation at the appropriate loci in T and B lymphocytes is associated with transcription and rearrangement of Ig and TCR genes, as well as with cell lineage–specific expression of CD4, CD8, and CD21 (12–15). When naive T cells differentiate to Th1 cells, but not to Th2 cells, DNase hypersensitive sites appear in the IFN-γ gene (16). Furthermore, the IFN-γ gene is methylated to a lesser extent in human and

*Department of Molecular Preventive Medicine, Graduate School of Medicine, The University of Tokyo, Tokyo 113-0033, Japan; †Department of Computational Biology, Graduate School of Frontier Sciences, The University of Tokyo, Chiba 277-8561, Japan; ‡Division of Nephrology, Department of Laboratory Medicine, Kanazawa University, Kanazawa 920-8641, Japan; §Department of Neurology, Graduate School of Medicine, The University of Tokyo, Tokyo 113-0033 Japan; ¶Department of Medical Genome, Graduate School of Frontier Sciences, The University of Tokyo, Chiba 277-8561, Japan; and ‖Department of Disease Control and Homeostasis, Faculty of Medicine, Kanazawa University, Kanazawa 920-8641, Japan

Received for publication August 20, 2012. Accepted for publication February 13, 2013.

This work was supported by a Grant-in-Aid for Scientific Research (C) and Core Research for Evolution Science and Technology of the Japan Science and Technology Agency. S.-i.H. was supported by the "Genome Information Big Bang" Global Center of Excellence project from the Ministry of Education, Culture, Sports, Science, and Technology of Japan.

The sequences presented in this article have been submitted to the National Center for Biotechnology Information Sequence Read Archive (http://www.ncbi.nlm.nih.gov/sra) under accession number SRP007816.

Address correspondence and reprint requests to Dr. Shin-ichi Hashimoto, Department of Molecular Preventive Medicine, Graduate School of Medicine, The University of Tokyo, Tokyo 113-0033, Japan. E-mail address: hashimot@m.u-tokyo.ac.jp

The online version of this article contains supplemental material.

Abbreviations used in this article: BM, bone marrow; CGI, CpG island; DMR, differentially methylated region; GO, Gene Ontology Consortium Database; MSCC, methyl-sensitive cut counting; P/I, PMA/ionomycin; SAGE, serial analysis of gene expression; TAE, Tris–acetate–EDTA; Tg, transgenic; TSS, transcription start site.

www.jimmunol.org/cgi/doi/10.4049/jimmunol.1202267

murine Th1 and CD8 effector cells than in naive and Th2 cells. In contrast, the IL-4 and IL-5 genes are less methylated in Th2 cells than in Th1 cells. Treatment of T cells in vitro with drugs that inhibit histone deacetylases or DNA methylation increases IL-4 and IFN-γ expression. Moreover, naive T cells from conditional Dnmt1-knockout mice, which lack DNA (cytosine-5-)-methyltransferase 1, express substantially more IFN-γ and IL-4 after Ag activation, an effect that appears to be mediated, at least in part, by demethylation of the *cis*-regulatory element (17). Recently, it was demonstrated that demethylation of the FOXP3 locus is pivotal for differentiation of $CD4^+CD25^+$ regulatory T cells (18) and that the CpG regions of cell type–specific genes (e.g., IL2RA, CTLA4, and CD40LG) in conventional human $CD4^+$ T cells and regulatory T cells are differentially methylated (19). A limiting DNA methylation affects the proliferative potential of Ag-specific $CD8^+$ T cells with moderate effects on their differentiation to effector and memory $CD8^+$ T cells (20). Additionally, methyl-CpG–binding domain protein 2–deficient mice display reduced memory $CD8^+$ T cell differentiation following acute viral infection (21).

These findings indicate that DNA methylation is crucial for memory T cell development and cytokine production. However, in T cells, the DNA methylation status of only a limited number of genes has been examined. The genome-wide DNA methylation status of memory $CD4^+$ T cells derived from Ag-stimulated naive cells remains unexplored. In this study, we investigated the gene-expression profiles and genome-wide DNA methylation status of naive and Ag-specific memory $CD4^+$ murine T lymphocytes.

Materials and Methods

Mice

BALB/c mice were purchased from Clea (Tokyo, Japan). OVA-specific TCR-transgenic (Tg) mice (DO.11.10; OVA-specific TCR Tg × $RAG2^{-/-}$ mice) were maintained under specific pathogen–free conditions.

Reagents

The anti–CD4-Pacific Blue (RM4-5), anti-CD62L mAb (MEL-14), anti–CD25-PE (7D4), PE-conjugated anti-CD4 mAb (GK1.5-PE), anti–CD44-bio (IM7), anti–CD69-bio (H1.2F3), anti–CD127-bio (A7R34), IFN-γ–FITC (XMG1.2), anti–IL-4–Alexa Fluor 647 (11B11), anti–TNF-α–PE/Cy7 (MP6-XT22), anti-mouse TCR DO11.10-PerCP/Cy5.5 (KJ1-26), and streptavidin-allophycocyanin were purchased from BD Pharmingen and eBioscience.

Generation of effector and memory $CD4^+$ T cells

OVA-specific naive $CD4^+$ T cells were isolated from the spleens of DO11.10-Tg mice. To generate effector cells, naive $CD4^+$ T cells were stimulated with 1 μg/ml an OVA peptide (residues 323–339; ISQAVHAAHAEINEAGRD; synthesized by Sigma Genosys, Hokkaido, Japan) plus allophycocyanin for 5 d in vitro (22). Five million of these cells were transferred i.v. into normal syngeneic BALB/c recipient mice. In most experiments, 4 wk after effector cell transfer, $KJ1^+$ cells from the spleens of recipient mice were sorted by FACSVantage (BD Pharmingen) and used as memory $CD4^+$ T cells.

Assays for cytokine production

Naive effector and memory $KJ\text{-}1^+CD4^+$ T cells were restimulated with PMA (20 ng/ml)/ionomycin (1 μg/ml) (P/I) and brefeldin A (10 μg/ml) for 5 h. Cells were then fixed (Cytofix buffer; BD Pharmingen), permeabilized, stained intracellularly with anti–IFN-γ Ab, anti–IL-4 Ab, or anti–TNF-α Ab or its isotype control, and analyzed using a Gallios Flow Cytometer (Beckman Coulter).

Methyl-sensitive cut counting library construction

The integrity of cDNA was confirmed using an Agilent 2100 Bioanalyzer prior to construction of the methyl-sensitive cut counting (MSCC) libraries. The protocol for MSCC library construction was modified slightly from that described previously (23).

Adapters A1 (5′-TTTCCACTACGCCTCCGCTTTCCTCTCTATGGGCAGTCGGTGATCCGAC-3′) and A2 (5′-CGGTCGGATCACCGACTGCCCATAGAGAGGAAAGCGGAGGCGTAGTGG-3′) contain a 5′ MmeI recognition site and a 5′-CG overhang; adapters B1 (5′-CGCCTTGGCCGTACAGCAGAGCTTACCGCAGAGAATGAGGAACCCGGGGCAG-3′) and B2 (5′-TTTCTGCCCCGGGTTCCTCATTCTCTGCGGTAAGCTCTGCTGTACGGCCAAGGCGNN-3′) contain a 3′-NN overhang and barcode (more information in Supplemental Table I), as described in the Applied Biosystems protocol. To construct the MSCC HpaII library, 1 μg genomic DNA isolated from $CD4^+$ T cells was mixed with 8 U HpaII (New England BioLabs) in 1× NEBuffer 1 in a 50-μl reaction volume and incubated at 37°C for 12 h. Another 8 U HpaII was added, and the mixture was incubated at 37°C for an additional 3 h. DNA was purified by phenol-chloroform extraction and ethanol precipitation and resuspended in 12.5 μl dH_2O. This 12.5-μl DNA solution was mixed with 1.5 μl a mixture containing 5 μM adaptor A1, 5 μM adaptor A2, and 10 U T4 DNA ligase (Invitrogen) before incubation at 16°C for 12 h. DNA was again purified by phenol-chloroform extraction and ethanol precipitation and resuspended in 8 μl dH_2O. This DNA was run on a 10% nondenaturing Tris–acetate–EDTA (TAE) polyacrylamide gel, and the 60–80-bp band was purified. After ethanol precipitation, the DNA pellet was resuspended in 70 μl a reaction mixture containing 14 U MmeI (New England BioLabs), 50 μM S-adenosyl methionine, and 1× NEBuffer 4. This mixture was incubated at 37°C for 12 h, after which DNA was again purified by phenol-chloroform extraction and ethanol precipitation and resuspended in 13 μl dH_2O. This DNA solution was mixed with 1 μl each 5.8 μM adaptor B1 and B2 and 10 U T4 DNA ligase, and the mixture was incubated at 16°C for 12 h. DNA was again purified and resuspended in 20 μl dH_2O. This DNA solution was mixed with 10 U DNA polymerase I (New England BioLabs), 33 μM 2′-deoxynucleoside 5′-triphosphate, and 1× NEBuffer and incubated at 16°C for 30 min. DNA was again purified and resuspended in 8 μl dH_2O. This DNA was run on a 9% nondenaturing TAE polyacrylamide gel, and the 120–140-bp band was purified. The purified DNA was then amplified by PCR using the primers 5′-CCACTACGCCTCCGCTTTCCTCTCTATGGGCAGTCGGTGAT-3′ and 5′-CTGCCCCGGGTTCCTCATTCTCT-3′. The 20-μl mixture for PCR contained 200 nM of each primer, 200 nM 2′-deoxynucleoside 5′-triphosphate, 1× PS buffer, and 1.25 U PrimeSTAR HS DNA polymerase (TaKaRa) and was run at 98°C for 30 s; 10 cycles at 98°C for 5 s, 62°C for 15 s, 72°C for 1 min; and then 72°C for 10 min. The PCR product was run on a 9% nondenaturing TAE polyacrylamide gel, and the 120–130-bp band was purified. The purified libraries were sequenced with the Applied Biosystems SOLiD4 system, following the manufacturer's protocol. The integrity of the cDNA was confirmed using an Agilent 2100 Bioanalyzer prior to construction of the MSCC libraries. A 1-ng sample of size-fractionated cDNA was used for sequencing reactions.

An MspI control library was constructed in the same manner as the HpaII library, with the following exceptions: in the first step, 100 U MspI (New England BioLabs) was used instead of HpaII, and NEBuffer 2 was used instead of NEBuffer 1, and no amplification was performed following gel purification. All HpaII libraries were normalized to 5 million.

SOLiD BioScope software (version 1.3) was used to determine methyl-sensitive restriction enzyme scores and map MSCC sequence reads (20 bp from the MmeI restriction site) to the mouse genome assembly (NCBI37/mm9). A DNA-methylation score was defined as the sum of tag sequence hits (a plus-strand tag and a minus-strand tag) for each restriction enzyme site, in the absence of repetitive sites, and normalized to 10^6 reads by the specific enzyme. To avoid inaccurate identification of methylation sites, differentially methylated regions (DMRs) were defined as those with a change from 0 tags (high-methylation group) to >10 tags (low-methylation group).

Generation and sequencing of the 5′-serial analysis of gene expression library

A newly developed 5′-end mRNA collection method (24) has extended the range of the original 5′-end serial analysis of gene expression (SAGE) technique. This method initially profiles 25-nucleotide 5′-SAGE tags using a novel strategy that incorporates the oligo-capping method. The 5′-SAGE tags are then ligated directly to a linker for sequencing. The purified libraries were sequenced with a Solexa system, according to the manufacturer's protocol (Illumina). The integrity of the cDNA was confirmed using an Agilent 2100 Bioanalyzer prior to construction of 5′-SAGE libraries. A 1-ng sample of size-fractionated cDNA was used for sequencing reactions with the Illumina GA, performed according to the manufacturer's instructions. We assigned unique tags to RefSeq genes (University of California, Santa Cruz, http/hgdownload.cse.ucsc.edu/goldenPath/mm9/database/) when the start position of the tag was within 500 bp upstream of the transcription start site (TSS), based on RefSeq annotation.